IIc. Application of the methods of calculation to reinforced concrete structures

Objekttyp: **Group**

Zeitschrift: **IABSE congress report = Rapport du congrès AIPC = IVBH Kongressbericht**

Band (Jahr): **5 (1956)**

PDF erstellt am: **12.07.2024**

Nutzungsbedingungen

Die ETH-Bibliothek ist Anbieterin der digitalisierten Zeitschriften. Sie besitzt keine Urheberrechte an den Inhalten der Zeitschriften. Die Rechte liegen in der Regel bei den Herausgebern.
Die auf der Plattform e-periodica veröffentlichten Dokumente stehen für nicht-kommerzielle Zwecke in Lehre und Forschung sowie für die private Nutzung frei zur Verfügung. Einzelne Dateien oder Ausdrucke aus diesem Angebot können zusammen mit diesen Nutzungsbedingungen und den korrekten Herkunftsbezeichnungen weitergegeben werden.
Das Veröffentlichen von Bildern in Print- und Online-Publikationen ist nur mit vorheriger Genehmigung der Rechteinhaber erlaubt. Die systematische Speicherung von Teilen des elektronischen Angebots auf anderen Servern bedarf ebenfalls des schriftlichen Einverständnisses der Rechteinhaber.

Haftungsausschluss

Alle Angaben erfolgen ohne Gewähr für Vollständigkeit oder Richtigkeit. Es wird keine Haftung übernommen für Schäden durch die Verwendung von Informationen aus diesem Online-Angebot oder durch das Fehlen von Informationen. Dies gilt auch für Inhalte Dritter, die über dieses Angebot zugänglich sind.

Ein Dienst der *ETH-Bibliothek*
ETH Zürich, Rämistrasse 101, 8092 Zürich, Schweiz, www.library.ethz.ch

http://www.e-periodica.ch

IIc1

Load distribution in right higway bridges

Lastverteilung bei geraden Brücken

Distribuição das cargas nas pontes-estrada rectas

Répartition des charges dans les ponts-route droits

G. LITTLE, M. Sc. R. E. ROWE, B. A.
P. B. MORICE, B. Sc., Ph. D.
Cement and Concrete Association
London

1. *Introduction.*

Accurate assessments of the effects of concentrated loads on medium span highway bridges have seldom been necessary in the past in Great Britain. This has been due to the fact that all practical loading conditions bridge loading which is a distributed loading. Recently, however, concentrated loads have been much heavier and more numerous necessitating have been catered for by the Ministry of Transport standard equivalent accurate assesments of their effects on existing bridges and on new bridges at the design stage. A new loading, the Ministry of Transport abnormal load, has therefore been proposed for trunk road bridge design in Great Britain which has the form shown in Figure 1 with a total weight of 180 tons. In certain cases the weight may be reduced to 120 tons, or even 80 tons, although the wheel positions remain the same.

The general distortion of a bridge deck carrying the abnormal load is a problem chiefly associated with short or medium spans because it is only on such bridges that the effects of a single vehicle, even of abnormal weight, can be greater than those of general traffic which is covered by the distributed design loading.

The analysis with which the experimental results given in this paper, have been compared is based upon linear elastic theory and is thus particularly applicable to prestressed concrete structures. The experimental work described is concerned with full scale and model prestressed bridges and perspex models of prestressed concrete type bridges.

2. *Methods of analysis.*

The short span wide slab bridge deck has been extensively studied in the United States of America between 1930 and 1940 by a number of people and this work has been reported in several excellent papers [1, 2, 3, 4].

Experimental work has been carried out chiefly on reinforced concrete slabs with good results and it is therefore reasonable to suppose that the theory applies also to prestressed concrete which more nearly satisfies the assumptions of isotropy.

Whilst short span bridges will, almost always, consist effectively of slabs, medium span bridges may appear in a variety of forms such

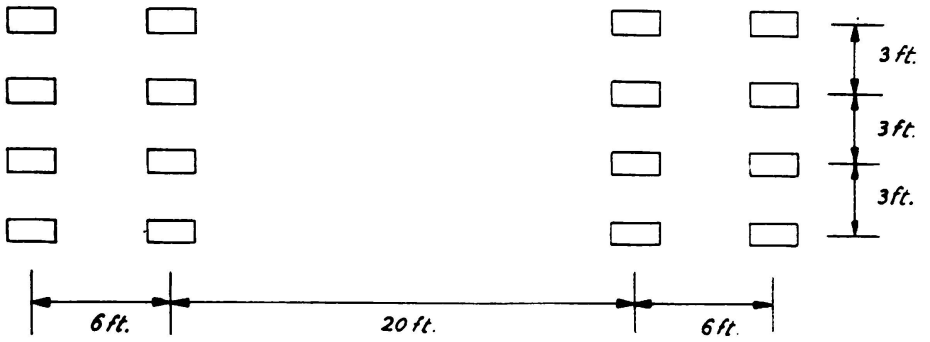

FIG. 1. Form of abnormal load

as slabs, grillages, Tee-beam and box-beam structures. It is not surprising that many methods have been advanced for their analysis when subjected to concentrated loading. These methods of analysis may be placed into three groups. The first separates the structure into a finite number of members in each direction, each with its own stiffness. The solution of the behaviour of the structure as a whole is then determined by solving the equations of compatibility which ensure continuity at the joints of the members.

The technique of solution of such systems of equations is well established in Southwell's relaxation technique. Janssonius [5] has developed this method for the study of transversely loaded grillages including the bridge deck case.

The second group of theories separates the main or primary members from the remainder of the structure and considers the effect of secondary cross-connexion between the main members. Hetenyi's [6] solution involving Fourier series is particularly elegant whilst there exist alternatives due to Pippart [7] and Leonhardt [8]. In the latter analysis the whole of the cross-connexion is replaced by a single centre span diaphragm of equivalent stiffness.

The third group of theories is that which reduces the actual structure to an equivalent distributed system in the two principal directions; a quasi orthotropic plate. The deflection of such a plate is governed by the generalized Lagrange equation

$$\rho_\rho \frac{\partial^4 w}{\partial x^4} + 2H \frac{\partial^4 w}{\partial x^2 \partial y^2} + \rho_E \frac{\partial^4 w}{\partial y^4} = p(x,y)$$

This method has been proposed by Guyon [9, 10], for torsionless grillages and for slabs and has been generalized by Massonet [11]. The quasi orthotropic plate analysis has the advantage that almost any structural form may be analysed in the same general terms. The method has become known as the «distribution coefficient method» due to the way in which it is convenient to apply the method to practical design.

A large number of the bridges which have to be built in practice are to provide a skew crossing. The analysis of skew bridges is a rather difficult problem and is not at present amenable to the same techniques as have been successfully used for right bridges. Some work has been reported [12, 13] on this problem and further work is in progress at the time of writing. Although no overall solution can be given it appears that the analysis of right bridges may be safely applied to bridges with up to about 15° skew.

3. *Theoretical analysis of the bridges under test.*

The analyses of Guyon and Massonnet have been considered to obtain the theoretical results for deflections and moments. The distribution coefficients, K, for deflections and longitudinal moments, were obtained from curves prepared by Guyon for a no-torsion grillage, and from curves prepared by the authors from Massonnet's tabulated values for a full torsion slab. The effect of ignoring Poisson's ratio in the analysis has been shown [14] to be negligible in the case of the coefficients K.

For the transverse bending moments, the equation

$$M_y = b \sum_{n=1}^{\infty} \mu_n H_n \sin \frac{n\pi x}{2a}$$

was used. H_n is the amplitude of the nth term in the Fourier series for the load, and μ_n is a distribution coefficient. Values of μ for a no-torsion grillage and a full-torsion slab were tabulated by Guyon and Massonnet respectively; additional values have been calculated by the authors and from these values curves have been prepared. The discrepancies between theoretical and experimental values for the transverse moments were found to be considerable and led to a consideration of the effect of Poisson's ratio in Guyon's analysis for a slab. The complete analysis is given elsewhere [14] but the analysis gives the following equation for μ_1:

$$\mu_1 = -\frac{1}{4\sigma \operatorname{sh}^2\sigma}\left\{\frac{[(1-\nu)\sigma\operatorname{ch}\sigma-(1+\nu)\operatorname{sh}\sigma]\operatorname{ch}\theta\psi-(1-\nu)\operatorname{sh}\sigma\,.\,\theta\psi\operatorname{sh}\theta\psi}{(3+\nu)\operatorname{sh}\sigma\operatorname{ch}\sigma-(1-\nu)\sigma}\right.\left\{[(1-\nu)\sigma\operatorname{ch}\sigma-(1+\nu)\operatorname{sh}\sigma]\operatorname{ch}\theta\beta-(1-\nu)\operatorname{sh}\sigma\,.\,\theta\beta\operatorname{sh}\theta\beta\right\}+$$

$$+\frac{[(1-\nu)\sigma\operatorname{ch}\sigma+2\operatorname{sh}\sigma]\operatorname{sh}\theta\psi-(1-\nu)\operatorname{sh}\sigma\,.\,\theta\psi\operatorname{ch}\theta\psi}{(3+\nu)\operatorname{sh}\sigma\operatorname{ch}\sigma+(1-\nu)\sigma}\left\{[(1-\nu)\sigma\operatorname{ch}\sigma+\right.$$

$$\left.+2\operatorname{sh}\sigma]\operatorname{sh}\theta\beta-(1-\nu)\operatorname{sh}\sigma\,.\,\theta\beta\operatorname{ch}\theta\beta\right\}+[(1-\nu)\sigma\operatorname{ch}\sigma-(1+\nu)\operatorname{sh}\sigma]\operatorname{ch}\theta\chi-$$

$$\left.-(1-\nu)\operatorname{sh}\sigma\,.\,\theta\chi\operatorname{sh}\theta\chi\right\}$$

where $\theta = \frac{b}{2a}$; $\sigma = \theta\pi$; $\beta = \frac{\pi_y}{b}$; $\psi = \frac{\pi\varepsilon}{b}$;

$\chi = \pi - /\beta - \psi/$; and ν = Poisson's ratio.

This equation was used to determine values of μ for a Poisson's ratio of 0.15, that assumed for prestressed concrete, and curves for the value of this coefficient have been prepared [14]. In the tests on bridge slabs the curves have been used to determine the theoretical transverse moments for this particular value of Poisson's ratio.

4. *Details of, and presentation of results from, the experimental investigations.*

(a) *Bridge slabs.*

A concrete slab, 57.8 × 46.25 × 1 in., post-tensioned to a residual stress of 850 lb/in². in both the longitudinal and transverse directions, was simply supported as a bridge slab and tests carried out for three different spans. The spans were taken to give values of the ratio $\frac{1/2 \times \text{breadth}}{\text{span}}$, denoted by θ, of 0.4, 0.5 and 0.6.

Loading consisting of one, two or four equal loads was applied to the slab and deflexions and strain measurements obtained. Electrical

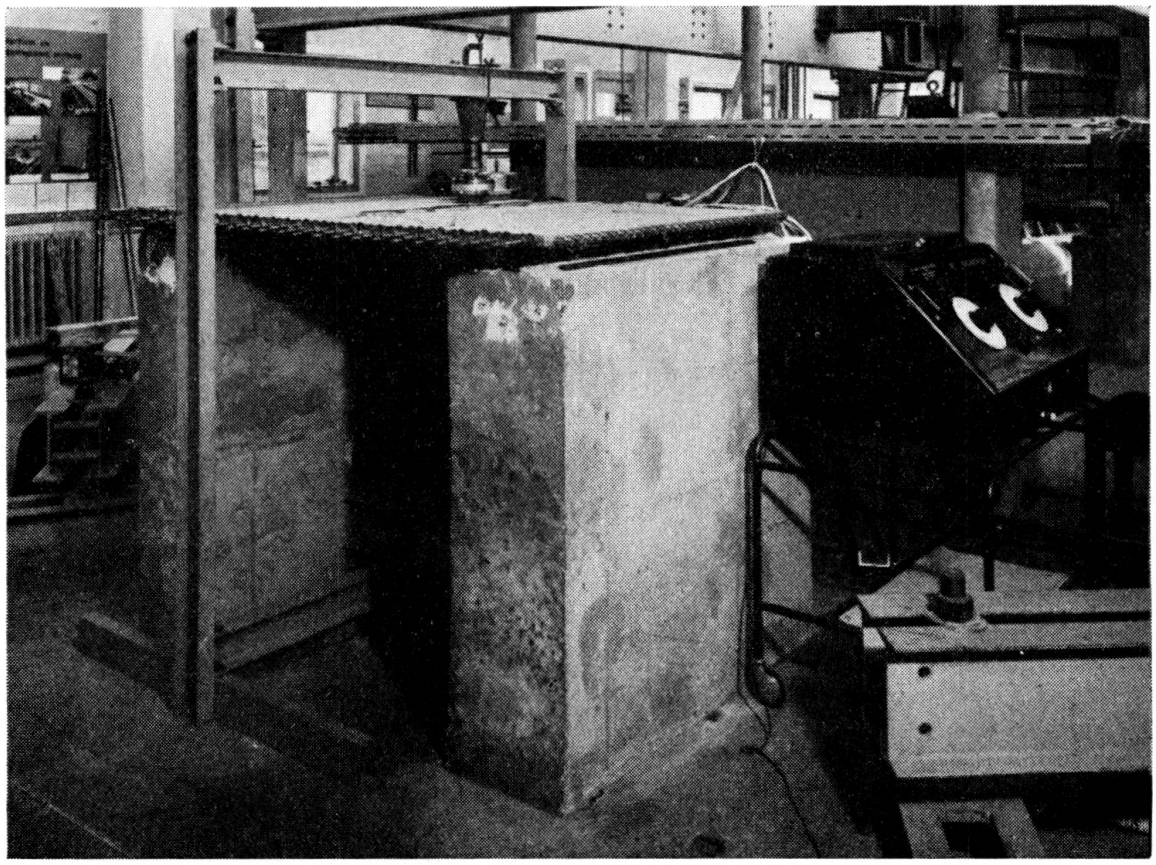

FIG. 2. General arrangement for testing bridge slabs

TABLE 1

Experimental distribution coefficients, K for deflections on the section under the load and discrepancies from the theoretical values

Position on slab	Experimental Values of K				Discrepancies from theoretical values (%)			
	Load Position				Load Position			
	0	b/4	b/2	3b/4	0	b/4	b/2	3b/4
b	0.924	1.106	1.280	1.556	1.2	2.9	- 1.3	0.4
3b/4	0.952	1.094	1.226	**1.369**	- 0.6	0.5	- 2.2	- 2.9
b/2	0.984	1.095	1.185	1.213	- 1.8	- 1.3	- 2.0	- 3.3
b/4	1.046	**1.074**	1.095	1.083	- 0.2	- 2.6	- 1.3	- 0.6
0	**1.084**	1.055	1.004	0.956	0.8	0.7	- 4.2	- 0.2
-b/4	1.046	**0.989**	0.910	0.850	- 0.2	1.4	1.0	1.4
-b/2	0.984	0.913	**0.826**	0.752	- 1.8	1.3	1.4	2.7
-3b/4	0.952	0.862	0.773	**0.677**	- 0.6	2.9	5.6	5.8
-b	0.924	0.819	0.728	0.639	1.2	5.0	9.5	9.2
	Slab No. 1: $\theta = 0.4$							
b	0.902	1.047	1.346	1.678	4.8	- 3.4	- 3.1	- 3.6
3b/4	0.934	1.077	1.309	**1.498**	0.6	- 4.6	- 3.3	- 4.6
b/2	1.001	1.125	**1.249**	1.275	- 0.1	- 3.0	- 3.3	- 5.8
b/4	1.062	**1.139**	1.115	1.058	- 1.3	- 1.5	- 3.9	6.2
0	**1.115**	1.068	0.985	0.906	0	- 0.8	- 1.5	- 2.4
-b/4	1.062	**0.967**	0.870	0.783	- 1.3	0 3	1.8	2.8
-b/2	1.001	0.885	**0.776**	0.710	- 0.1	3.5	6.1	12.2
-3b/4	0.934	0.824	0.729	**0.648**	0.6	8.1	15.1	21.3
-b	0.902	0.790	0.690	0.603	4.8	15.7	25.0	32.9
	Slab No. 2: $\theta = 0.5$							
b	0.831	1.044	1.362	**1.760**	5.2	- 3.8	- 6.6	- 9.3
3b/4	0.894	1.101	1.359	**1.597**	0.8	- 4.2	- 6.3	- 8.7
b/2	1.004	1.178	**1.339**	1.331	0.4	- 3.4	- 4.4	- 7.8
b/4	1.105	1.210	1.158	1.078	- 1.3	- 2.0	- 5.3	- 6.6
0	**1.179**	1.085	0.963	0.848	- 0.7	- 3.0	- 3.7	- 4.5
-b/4	1.105	**0.951**	0.827	0.740	- 1.3	- 0.4	3.2	8.4
-b/2	1.004	0.837	**0.733**	0.654	0.4	4.5	12.5	21.4
-3b/4	0.894	0.742	0.648	**0.585**	0.8	9.2	20.2	40.0
-b	0 831	0.676	0.584	0.528	5.2	22.2	33.1	59.0
	Slab No. 3: $\theta = 0.6$							

resistance foil gauges, of 1 in. gauge length, were used to obtain the strain readings. Figure 2 shows the test specimen, the loading device and the strain recorder. The modulus-time curve for the slab was determined by applying a line load over the complete width of the slab and observing deflections.

The experimental «mean» deflection and longitudinal moments were derived by applying Simpson's rule to the transverse profiles for deflections and moments; the experimental values of the distribution coefficients K, were then found from the measured «mean» and actual values. Table 1 gives the experimental values of K for deflections for a single concentrated load applied to each slab and the percentage discrepancies from the theoretical values. Each set of values of K shows symmetry about the marked diagonals illustrating that the reciprocal theorem held for the slabs. The discrepancy of the actual from the theoretical values is of the order of 2 per cent under the load, for zero eccentricity, increasing to 9 per cent for an eccentricity of 3b/4.

Table 2 gives some typical experimental values of K for longitudinal moments and the percentage discrepancies from the theoretical values for both single and double loads. These discrepancies are greater than those found for deflections but decrease as the number of loads increases. The local effects inherent in this type of loading cause a disturbance of the true distribution properties; the «mean» moment is invariable for any given load and hence the local effects cause an increase in the values of K in the region of the load and a consequent decrease in the values away from the load. This is clearly shown in Figure 3 where the theoretical and experimental transverse profiles for the values are given for both a single and two equal loads. Table 3 compares theoretical and experimental values K for longitudinal moments in the loaded zone for four equal applied loads applied to the third slab. The discrepancy between theoretical and experimental values is of the order of 10 per cent and is thus in agreement with Guyon's suggestion that, for practical loadings, it is necessary to increase the theoretical values by 10 to 15 per cent to obtain the actual.

In all the tests from which the above results were derived, the theoretical and experimental «mean» effects were in excellent agreement.

For the transverse moments Table 4 compares the theoretical and experimental moments at various points on the second slab for various load positions. Similar tables were obtained for the other slabs but are not given here. The experimental moments were derived from the measured strains and modulus on the assumption that Poisson's ratio, ν, was 0.15. This assumption was justified in that the experimental moments at the edges of the slabs were then zero. From the table it can be seen that considerable errors arise if no account is taken of Poisson's ratio in the theoretical analysis but, if allowance is made for this effect, greater accuracy is attained in estimating the actual moments for any disposition of the loads. This is also shown in Table 5 which compares theoretical and experimental moments at various points on the third slab when four equal loads were applied. This type of loading is analogous to that of the Ministry of Transport abnormal load.

TABLE 2

Experimental distribution coefficients, K, for longitudinal moments on the section under the load and discrepancies from the theoretical values

Position on slab	Single load							
	Experimental Values of K				Discrepancies from theoretical values (%)			
	Load Position				Load Position			
	0	b/4	b/2	3b/4	0	b/4	b/2	3b/4
b	0.754	0.940	1.333	1.943	- 12.4	- 14.1	- 4.0	11.6
3b/4	0.767	0.952	1.359	1.935	- 17.3	- 15.7	0.4	23.3
b/2	0.949	1.220	1.824	1.388	- 5.1	5.2	41.7	2.5
b/4	1.134	1.608	1.190	0.972	5.3	39.1	2.6	- 13.9
0	1.743	1.207	0.979	0.840	56.3	12.1	- 2.3	- 9.5
-b/4	1.134	0.850	0.719	0.619	5.3	- 11.8	- 15.9	- 18.8
-b/2	0.949	0.739	0.651	0.558	- 5.1	- 13.5	- 11.0	- 11.8
-3b/4	0.767	0.611	0.536	0.474	- 17.3	- 19.8	- 15.3	- 11.2
-b	0.754	0.596	0.536	0.476	- 12.4	- 27.2	- 2.9	4.8
	Slab No. 2: $\theta = 0.5$							
Loads at	Two equal loads							
	$\frac{b}{8}, \frac{-b}{8}$	$0, \frac{b}{4}$	$\frac{b}{4}, \frac{b}{2}$	$\frac{b}{2}, \frac{3b}{4}$	$\frac{b}{8}, \frac{-b}{8}$	$0, \frac{b}{4}$	$\frac{b}{4}, \frac{b}{2}$	$\frac{b}{2}, \frac{3b}{4}$
b	0.753	0.860	1.121	1.654	- 2.5	- 12.1	- 9.7	5.8
3b/4	0.775	0.883	1.130	1.713	- 8.3	- 14.2	- 8.9	17.5
b/2	0.945	1.097	1.481	1.574	1.7	1.5	20.7	18.9
b/4	1.194	1.416	1.422	1.067	13.0	26.8	24.0	- 6.8
0	1.486	1.426	1.095	0.894	35.0	30.1	5.3	- 7.3
-b/4	1.194	0.976	0.796	0.662	13.0	- 5.5	- 12.8	- 18.2
-b/2	0.945	0.819	0.700	0.598	1.7	- 11.8	- 11.8	- 12.3
-3b/4	0.775	0.676	0.583	0.507	- 8.3	- 19.9	- 16.5	- 13.2
-b	0.753	0.664	0.556	0.486	- 2.5	- 14.0	- 11.3	- 3.3
	Slab No. 2: $\theta = 0.5$							

TABLE 3

Slab No. 3: *Theoretical and experimental distribution coefficients, K, for longitudinal moments in the region of the loads for four equal applied loads*

Position on section		b/2	b/4	0	-b/4
Equal loads at ... ... $\pm$ b/8, $\pm$ 3b/8	Theoretical	1.012	1.081	1.107	1.081
	Experimental	1.096	1.080	1.227	1.080
Equal loads at ... ... b/2, b/4, 0, -b/4	Theoretical	1.106	1.133	1.107	1.028
	Experimental	1.160	1.174	1.249	0.990

TABLE 4

Slab No. 2: $\theta = 0.5$ — *Comparison of theoretical and experimental transverse bending moments (in. lb/in.) at various points for unit applied load.*

Transverse Moment at		a			0.688a			0.376a on longitudinal φ		
Loaded Transverse Section	Load Position	Theortical $\nu = 0.15$	Experimental	Theortical $\nu = 0$	Theortical $\nu = 0.15$	Experimental	Theortical $\nu = 0$	Theortical $\nu = 0$	Experimental	Theortical $\nu = 0.15$
a	0	0.2175	0.2174	0.2583	0.1029	0.0974	0.1238	0.0300	0.0338	0.0395
	b/4	0.0377	0.0557	0.0698	0.0349	0.0532	0.0595	0.0250	0.0243	0.0353
	b/2	- 0.0219	—	0.0049	- 0.0139	0.0227	0.0078	- 0.0015	0.0123	0.0095
	3b/4	- 0.0534	- 0.0260	- 0.0318	- 0.0432	- 0.0172	- 0.0253	- 0.0221	- 0.0105	- 0.0126
	b/8, -b/8	0.1100	0.1450	0.1380	0.0665	0.0926	0.0900	0.0285	0.0368	0.0385
	0, b/4	0.1273	0.1481	0.1640	0.0689	0.0827	0.0917	0.0275	0.0362	0.0374
	b/4, b/2	0.0076	0.0367	0.0374	0.0105	0.0431	0.0337	0.0118	0.0180	0.0224
	b/2, 3b/4	- 0.0377	- 0.0136	- 0.0135	- 0.0286	- 0.0047	- 0.0088	- 0.0118	—	- 0.0016
Transverse Moment at		b/4			b/2			3b/4 on central transverse section		
a	3b/4	- 0.0633	- 0.0428	- 0.0168	- 0.0023	0.0115	0.0286	0.1658	0.1560	0.2005
	b/2	0.0266	0.0490	0.0590	0.2071	0.2155	0.2391	0.0306	0.0396	0.0520
	b/4	0.2017	0.2298	0.2566	0.0376	0.0542	0.0683	- 0.0063	0.0076	0.0129
	0	0.0366	0.0594	0.0723	- 0.0094	0.0109	0.0158	- 0.0169	- 0.0028	- 0.0033
	-b/4	- 0.0089	0.0104	0.0133	- 0.0249	- 0.0055	- 0.0080	- 0.0215	- 0.0067	- 0.0133
	-b/2	- 0.0359	- 0.0114	- 0.0157	- 0.0365	- 0.0125	- 0.0206	- 0.0250	- 0.0105	- 0.0153
	-3b/4	- 0.0490	- 0.0240	- 0.0338	- 0.0404	- 0.0173	- 0.0287	- 0.0235	- 0.0118	- 0.0177
	0, b/4	0.1191	0.1741	0.1645	0.0141	0.0432	0.0421	- 0.0192	0.0063	0.0048
	b/2, b/4	0.1141	0.1652	0.1578	0.1224	0.1394	0.1587	0.0122	0.0246	0.0325
	b/2, 3b/4	- 0.0184	0.0159	0.0211	0.1024	0.1185	0.1339	0.0982	0.1209	0.1263
	b/8, -b/8	0.0665	0.0926	0.1036	- 0.0015	0.0195	0.0230	—	—	—

Sign convention: Positive denotes a sagging moment.

For the slabs with values of θ of 0.5 and 0.6, the enveloping curves for the ratio of the maximum transverse moment at any point to the maximum longitudinal moment at the centre of the slab for a load traversing the central transverse section are given in Figures 4 (a) and (b). The maximum transverse moment is appreciably constant

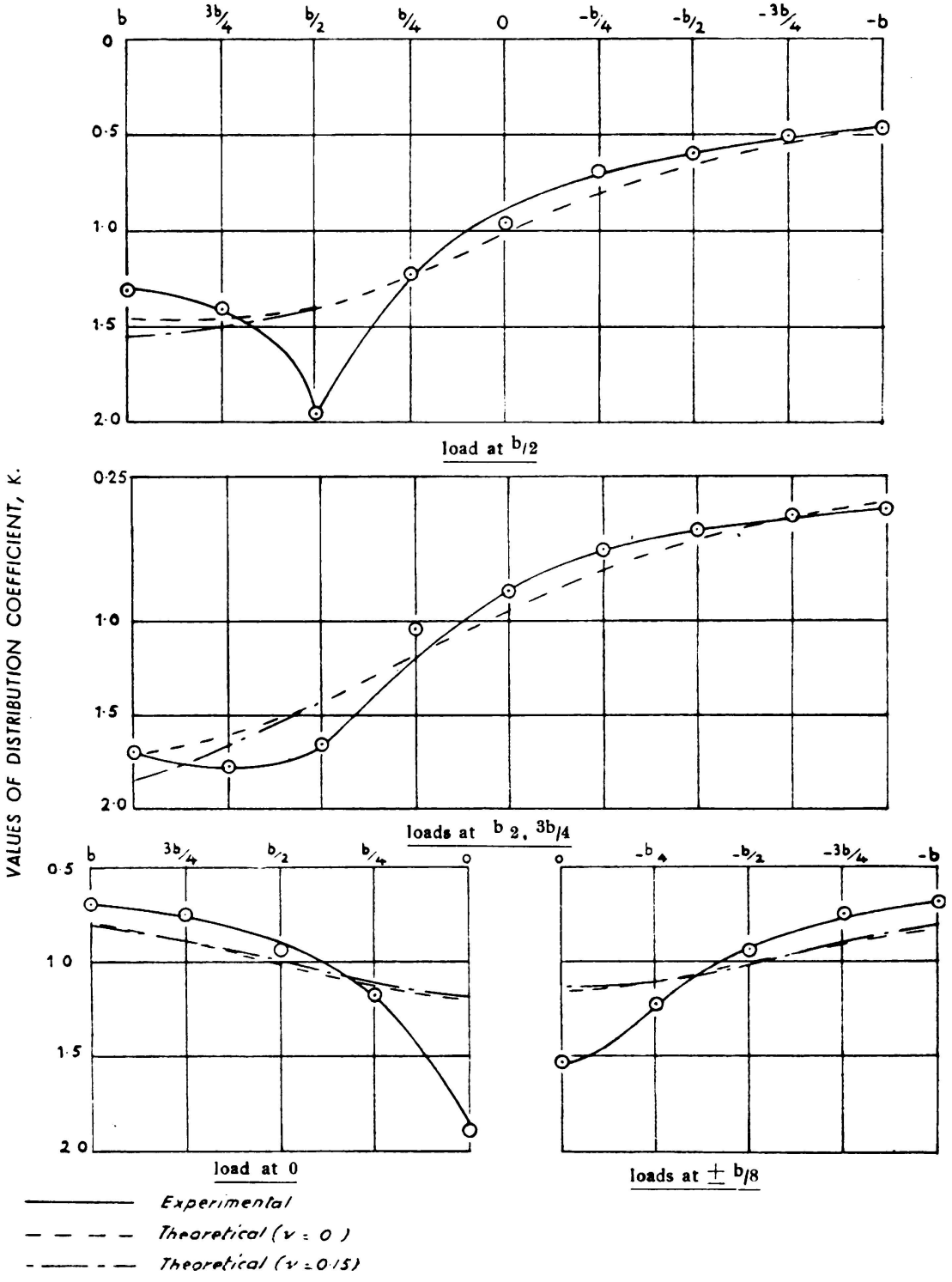

FIG. 3. Slab No. 3 – Comparison of theoretical and experimental profiles for coefficient, K

between $^{b}/_{2}$ and $-^{b}/_{2}$ and is always overestimated by the theoretical analysis assuming a Poisson's ratio of 0.15. In the case of four equal applied loads, the maximum transverse moment at the centre of the slab was 31.6 per cent of the corresponding longitudinal moment and the variation in the percentage as the load traversed the span is as shown in Figure 4 (c). Again the theoretical analysis assuming a Poisson's ratio of 0.15 accurately assesses the spanwise variation in the transverse moments.

From the tests it is apparent that the load distribution analysis, assuming a Poisson's ratio of zero, gives accurate assessments of the deflections and longitudinal moments for bridge slabs in prestressed concrete. For deflections the accuracy is of the order of 5 per cent for values of θ of 0.4 and 0.5 and 9 per cent for a value of θ of 0.6. These figures apply in the loaded region and increase to the maximum values given with increasing eccentricity. For practical forms of loading it is necessary to increase the theoretical values for the longitudinal moments by 10 per cent to obtain the actual.

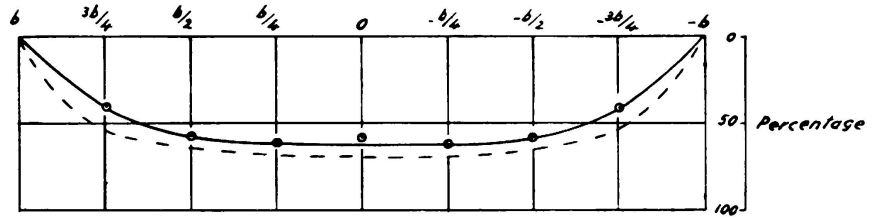

(a) Slab N° 2: θ = 0·5 - Enveloping curves for $\frac{M_y}{M_x \text{ at } 0 \text{ for load at } 0}$ for a load traversing transverse $\mathbb{C}$

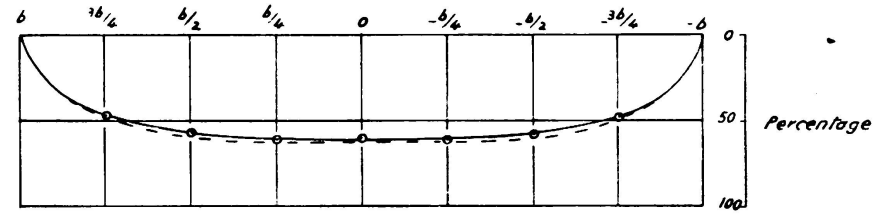

(b) Slab N°3: θ 0·6 - Enveloping curves for $\frac{M_y}{M_x \text{ at } 0 \text{ for load at } 0}$ for a load traversing transverse $\mathbb{C}$

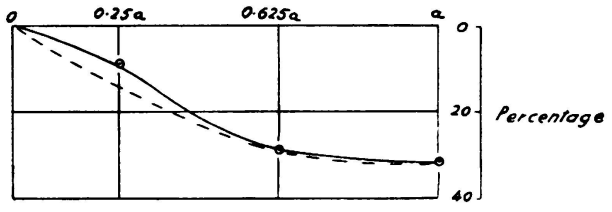

(c) Slab N°3: θ = 0·6 - Enveloping curves for $\frac{My \text{ on } \mathbb{C}}{\text{max. } M_x \text{ at centre}}$ for four equal loads traversing span

—— Experimental

- - - - Theoretical (ν = 0·15)

FIG. 4. Enveloping curves for distribution of transverse bending moment, M_y

TABLE 5

Slab No. 3 — *Comparison of theoretical and experimental transverse bending moments (in. lb/in.) for four equal loads giving unit total applied load*

Loads and moments on transverse section at		Load Positions	Transverse Moment at	Theoretical $\nu = 0$	Experimental	Theoretical $\nu = 0.15$
	a	$\pm$ b/8, $\pm$ 3b/8	b/2	—	—	—
			b 4	0.0430	0.0659	0.0673
			0	0.0456	0.0697	0.0757
			- b 4	0.0430	0.0659	0.0673
		b/2, $\pm$ b/4 and 0	b/2	0.0423	0.0762	0.0652
			b/4	0.0569	0.0860	0.0869
			0	0.0572	0.0858	0.0868
			- b 4	0 0426	0.0653	0.0638
	0.625 a	$\pm$ b/8, $\pm$ 3b/8	0	0.0393	0.0612	0.0671
		b/2, $\pm$ b/4, 0	0	0.0507	0.0715	0.0788
	0.25 a	$\pm$ b/8, $\pm$ 3b/8	0	0.0127	0.0143	0.0261
		b/2, $\pm$ b/4, 0	0	0.0236	0.0248	0.0373

TABLE 6

Prototype. *Comparison of distribution coefficients for load less than the transverse working load*

$\theta = 0.684$ and $\sqrt{\alpha} = 0.78$

Position of load	Distribution coefficients at mid-span								
	-b	$\frac{-3b}{4}$	$\frac{-b}{2}$	$\frac{-b}{4}$	0	$\frac{b}{4}$	$\frac{b}{2}$	$\frac{3b}{4}$	b
Mid-span									
$\gamma = 0$									
Experimental	0.62	0.81	1.02	1.22	1.26	1.22	1.02	0.81	0.62
Theoretical	0.63	0.82	1.02	1.20	1.27	1.20	1.02	0.82	0.63
$\gamma = 0.39b$									
Experimental	0.36	0.45	0.61	0.83	1.08	1.32	1.41	1.43	1.41
Theoretical	0.27	0.42	0.61	0.85	1.10	1.32	1.43	1.41	1.37

In the case of the transverse moments considerable errors occur if Poisson's ratio is assumed to be zero. However the introduction of a Poisson's ratio in the theoretical analysis enables an accurate assessment of the moments for any configuration of loads. The maximum transverse moment occurring in a slab is greater than that normally allowed for. For four equal applied loads the maximum transverse moment was 31.6 per cent of the corresponding longitudinal moment. This case may be considered as analogous to one axle of the Ministry of Transport abnormal load. In practice it will always be possible to place one bogie, i. e. two axles, of this load on any bridge and it is estimated that the maximum transverse moment will then lie between 25 and 30 per cent of the corresponding longitudinal moment at the centre of the slab. The disposition of loads to give the maximum transverse moment will be such that one internal line of wheels of the abnormal load is on the longitudinal centreline.

The theoretical analysis for transverse moments assuming $\nu = 0.15$ can be accurately used to determine the required amount of transverse prestressing necessary and its distribution along the span.

(b) *Tests for the distribution of load in a prestressed concrete highway bridge and in a model of the bridge.*

The deck of the bridge consisted of twenty precast prestressed beams placed side by side. These were stressed together transversely to form a slab with a skew of 15 degrees. The span was 33 ft 6 in. and the width 25 ft 0 in. A uniform transverse prestress of 70 lb/sq. in. was applied only over the central 20 ft 0 in. of the span. The initial prestress plus dead load stresses in the beams were 0 lb/sq. in and 1,615 lb/sq. in. at the extreme fibres. The Ministry of Transport abnormal load trailer was used for loading the bridge. Only one bogie could be on the bridge at one time and the load on it could be varied in fixed increments between 26.7 tons and 90 tons.

The distribution of deflection and of strain was measured along the transverse sections $^1/_4$ and $^1/_2$-span using 0.0001 in. deflection gauges and demountable mechanical strain gauges.

The centroid of the loading bogie was positioned successively at $^1/_4$ and $^1/_2$-span at eccentricities of 0 and 4 ft 10 $^1/_2$ in. or 0.39b and new zero values were recorded at each increment of load.

The test was discontinued at a load of 72 tons when a sudden reduction in the edge coeficient and corresponding increases in the coefficients for the adjacent beams showed a radical change in the distribution properties. A subsequent analysis of transverse moments by the μ-coefficient method showed, in fact. that the transverse strength of the bridge was equivalent only to 17 tons and 20 tons for the two eccentricities. Cracks had, therefore, occurred between the beams from the beginning and the distribution properties had deteriorated continuously. If this cracking had not occurred the corresponding longitudinal working loads would have been 96 tons and 85 tons respectively. The comparison between the practical and theoretical results is made after the description of further tests on a model of the bridge.

The model was constructed to $^1/_4$-scale, Figure 5, details such as surfacing and footpaths being omitted since neither had much effect on the distribution behaviour in the actual bridge. The initial stress conditions were reproduced in the model though with a slight reduction in the transverse prestress because of anchorage and friction losses. Ultimate conditions could not be reproduced as neither cable size and position nor dead weight stresses could be scaled down effectively.

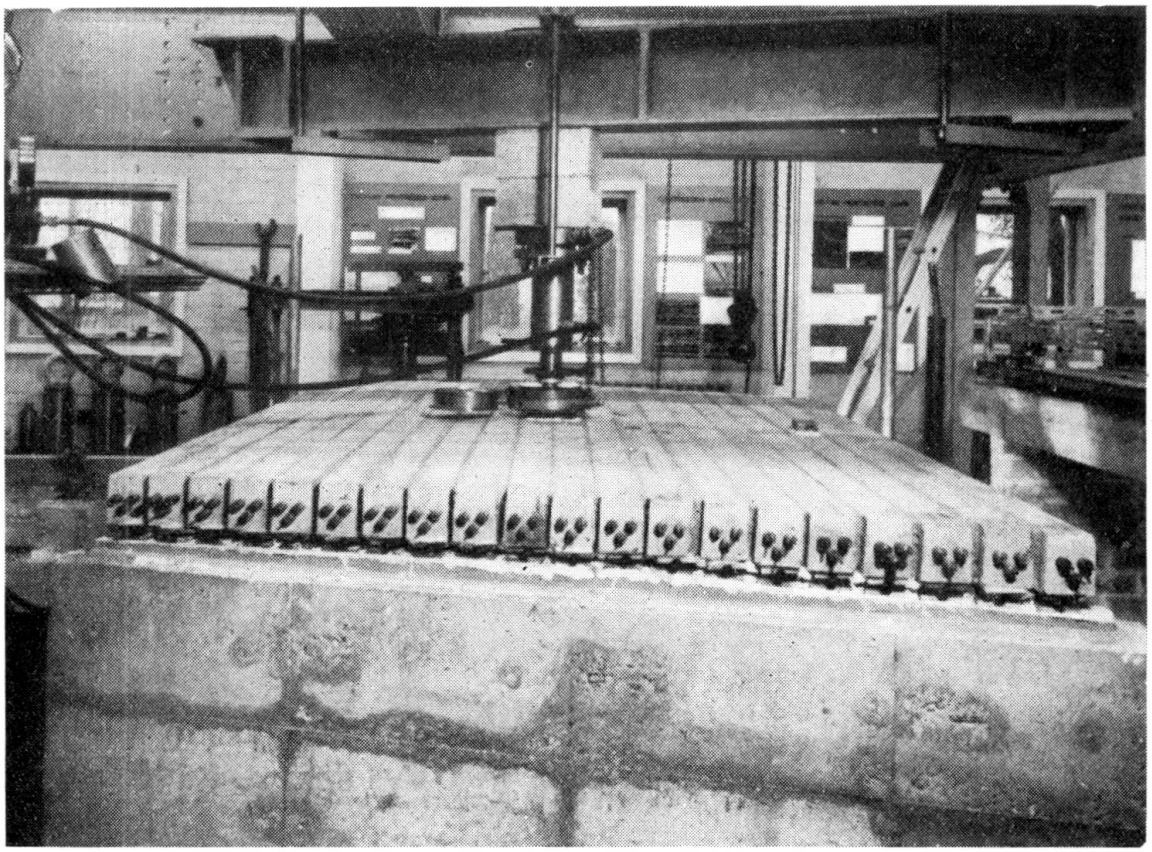

FIG. 5. Model bridge under test

Initial tests were made with a single concentrated load placed at mid-span with an eccentricity of either 0 or 3b/4. Figure 6 shows that the efficiency of distribution is controlled by the transverse strength of the bridge. The transverse working load for zero eccentricity as calculated from the μ-coefficient analysis is indicated in Figure 6 and gives a good estimate of the actual value. The transverse working loads were 1 ton and 1.35 tons. The corresponding longitudinal working loads if no cracking had occurred between the beams were 5.25 and 2.60 tons for $e = 0$ and $e = 3b/4$ respectively. Actually at these loads the most heavily loaded beams were over stressed by 22 per cent and 8 per cent respectively equivalent to tensile stresses of 350 lb/sq. in. and 130 lb/sq. in. This comparison confirms that the greatest transverse moment and the least maximum longitudinal moment occur for the minimum eccentricity of load. The comparison has been made for the values of θ and α found by experiment and given later.

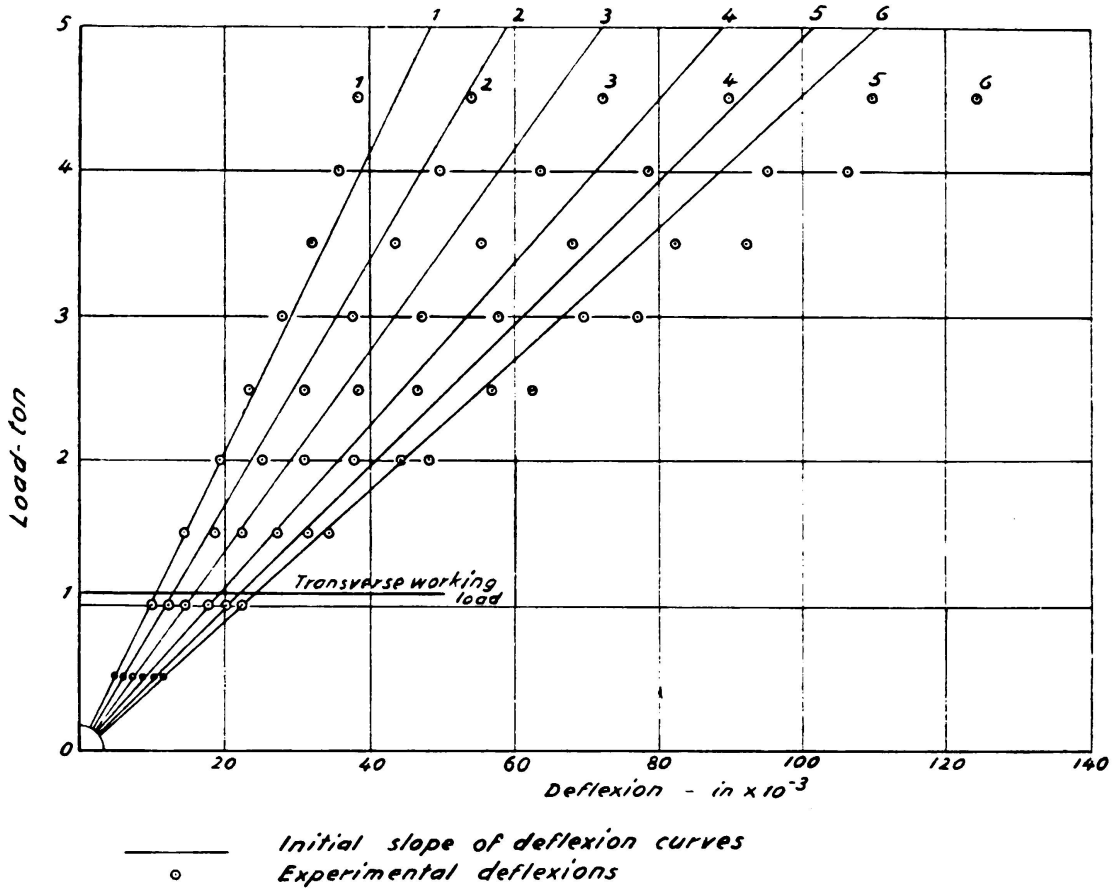

FIG. 6. Deflection curves for central concentrated load on model bridge

The bogie of the Ministry of Transport abnormal load trailer was reproduced to $^1/_4$-scale and further tests were made for mid-span loading at resultant eccentricities of e = 0 and e = 1 ft $2\,^5/_8$ in. or 0.39b. Again the transverse working loads controlled the distribution and were 1.10 tons and 1.25 tons for the two eccentricities. If no cracks had developed between the beams the corresponding longitudinal working loads would have been 5.75 tons and 5.35 tons respectively. The extent of the transverse cracking is indicated in Figure 7 where a comparison is made with the equivalent maximum longitudinal strains.

The measured strains were converted into bending moments by the use of moment-rotation curves found from a control test on a single beam. The working load of this beam was found to be equal to 650 lb and the value of Young's modulus $E = 5.76 \times 10^6$ lb/sq. in. As an accuracy of 15 per cent was assumed in assessing bending moments, and allowing for this, the comparison between the distribution of deflections and of moment was acceptable.

An elastic theory could only be expected to be valid if transverse cracking did not occur as an undefinable deterioration in distribution takes place under loads greater than the transverse working load. The following comparison with theory has, therefore, been made only for the initial linear part of the load and deflection curves as indicated in

Figure 6. In this range θ is constant since i = j. It had to be assumed that α would have a value less than unity if the total transverse prestress were insufficient to induce the same torsional and shear properties as an equivalent monolithic slab.

In determing θ, which is equal to b/2a in the linear range, 2a was taken as the length of span over which the transverse prestressing force was applied. The value of θ was thus 0.684 for the bridge and the model. From the interpolation expression $K_\alpha = K_o + (K_1 - K_o)\sqrt{\alpha}$ it was seen that α was, in fact, less than unity and that a value of 0.72 for α satisfied all conditions of loading in the model whilst a value of 0.78 described the behaviour of the bridge. The comparisons are made in Tables 6 and 7 which show the excellent agreement. The common value of θ showed that the bridge had been faithfully reproduced in the model whilst the higher value of α for the bridge was explained by the smaller transverse prestress in the model.

If the amount of transverse prestress in the bridge had been greater then the effective value of α would have been extended.

An ultimate load test on the model with the load at an eccentricity of 0.39b showed an ultimate load of 9 tons when fourteen of the beams failed at mid-span. The load factor was thus, 1.68 on a working load based on an uncracked transverse section. The better grouting and higher effective value of α would cause a higher load factor for the bridge.

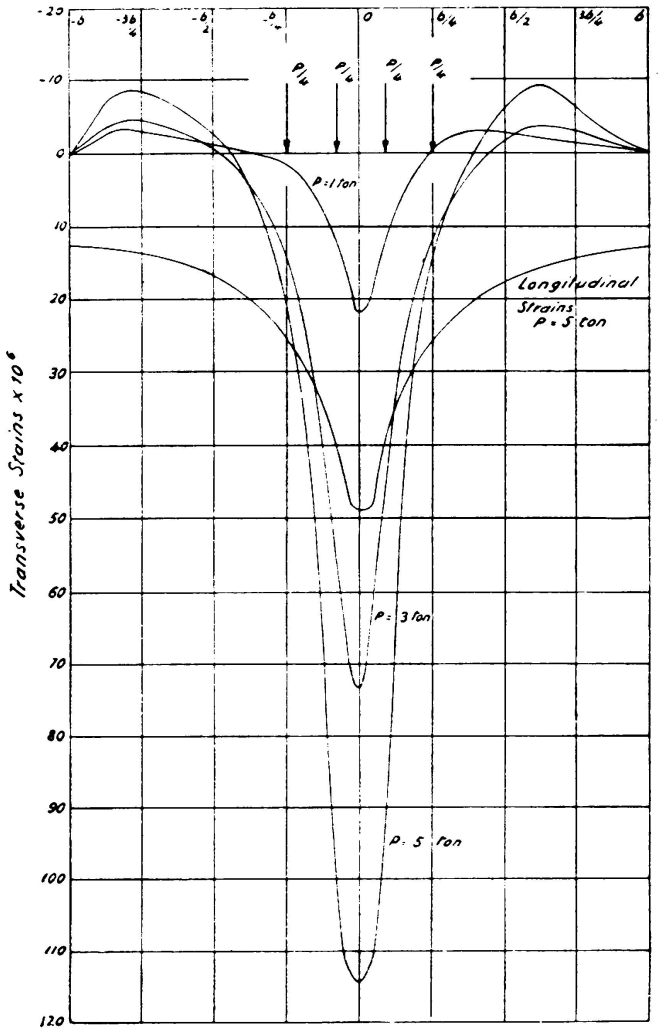

FIG. 7. Transverse strain profiles in model bridge

(c) *The distribution of load in a multi-webbed box-section bridge.*

The load distribution properties of a multi-webbed box-section bridge were found from the behaviour of a small xylonite model having the dimensions shown in Table 8 and illustrated in Figure 8. Transverse deflection profiles were recorded at each line of diaphragms for different positions of a single load concentrated on an area $2\frac{1}{2}$ in. $\times$ 1 in. The

TABLE 7

Model. *Comparison of distribution coefficients for load less than the transverse working load.*

$\theta = 0.684$ and $\sqrt{\alpha} = 0.72$

Position of load	Distribution coefficients at mid-span								
	-b	$\frac{-3b}{4}$	$\frac{-b}{2}$	$\frac{-b}{4}$	0	$\frac{b}{4}$	$\frac{b}{2}$	$\frac{3b}{4}$	b
Mid-span									
a) Concentrated load									
$\gamma = 0$									
Experimental	0.59	0.77	0.99	1.23	1.43	1.23	0.99	0.77	0.59
Theoretical	0.51	0.77	1.00	1.25	1.37	1.25	1.00	0.77	0.51
$\gamma = \frac{3b}{4}$									
Experimental	0.09	0.16	0.26	0.44	0.70	1.10	1.72	2.27	2.63
Theoretical	0.02	0.13	0.27	0.47	0.76	1.17	1.69	2.20	2.62
b) M. O. T. load									
$\gamma = 0$									
Experimental	0.57	0.81	1.03	1.20	1.34	1.20	1.03	0.81	0.57
Theoretical	0.56	0.79	1.02	1.23	1.31	1.23	1.02	0.79	0.56
$\gamma = 0.39b$									
Experimental	0.27	0.42	0.62	0.87	1.07	1.27	1.44	1.49	1.32
Theoretical	0.22	0.41	0.62	0.89	1.15	1.36	1.42	1.38	1.28
	Distribution coefficients at quarter-span								
Mid-span									
a) Concentrated load									
$\gamma = 0$									
Experimental	0.53	0.80	1.02	1.25	1.37	1.25	1.02	0.80	0.53
Theoretical	0.51	0.77	1.00	1.25	1.37	1.25	1.00	0.77	0.51
$\gamma = \frac{3b}{4}$									
Experimental	-0.11	0.04	0.22	0.47	0.75	1.16	1.71	2.32	2.94
Theoretical	0.02	0.13	0.27	0.47	0.76	1.17	1.69	2.20	2.62
b) M. O. T. load									
$\gamma = 0$									
Experimental	0.58	0.81	1.03	1.22	1.29	1.22	1.03	0.81	0.58
Theoretical	0.56	0.79	1.02	1.23	1.31	1.23	1.02	0.79	0.56
$\gamma = 0.39b$									
Experimental	0.09	0.31	0.60	0.90	1.14	1.32	1.43	1.50	1.54
Theoretical	0.22	0.41	0.62	0.89	1.15	1.36	1.42	1.38	1.28

TABLE 8

Dimensions of box-section bridge model

Span	18 in.
Width	9 in.
Number of webs:	
Longitudinal	7
Transverse	7
Thickness of webs	$\frac{1}{8}$ — in.
Thickness of slabs	1/16 in.

corresponding longitudinal and transverse strains were measured by electrical resistance strain gauges.

The modulus of elasticity E was determined by applying equal loads at the third points of a xylonite beam with the same span as the model and measuring the resulting mid-span strains. The total strain after four equal increments of load, with three minutes allowed between

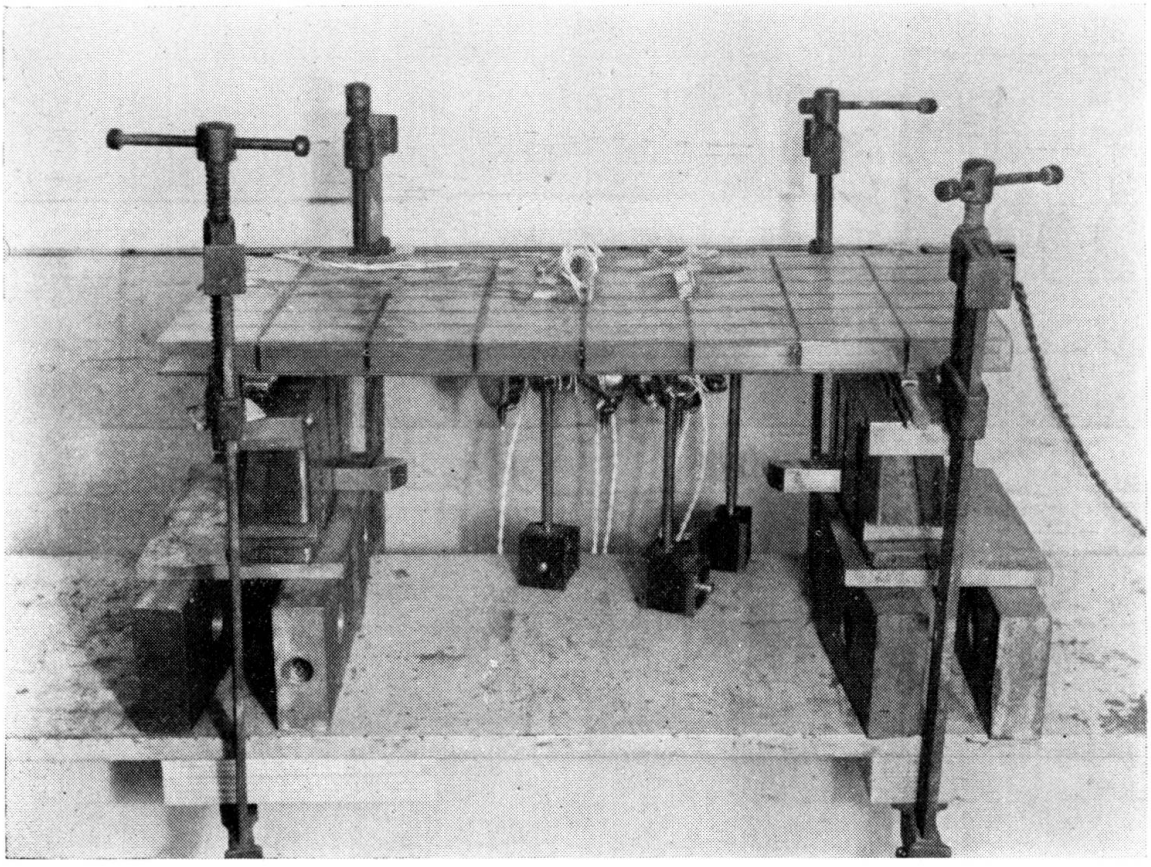

FIG. 8. Box-section bridge in test position

each increment for creep, was equal to the total strain after an interval of twelve minutes when the total load was applied instantaneously. The modulus E was calculated as the ratio of the maximum stress and the maximum strain recorded and its value was 33.33×10^4 lb/sq. in.

The shear modulus, G, was found by applying a known torque at the ends of the beam which was now supported vertically to obviate the effects of self bending. The angle of twist was measured by deflectometer readings at two sections, six inches apart. All significant creep had occurred after 15 minutes. The value of G was then equal to 11.7×10^4 lb/sq. in.

The value of Poisson's ratio was 0.42. The makers of the material gave an average value of 0.40.

The comparison between the theoretical and the experimental coefficients, K, for deflection is made in Table 9. Small variation was caused

TABLE 9

Comparison between the "mean" experimental distribution coefficients, K, for deflection and the theoretical coefficients

Beam Position	Section	Load Position						
		1	2	3	4	5	6	7
4 (Central Beam)	2 (1/6 span)	0.96	1.00	1.01	1.03	—	—	—
	3 (1/3 span)	0.96	1.00	1.01	1.04	—	—	—
	4 (1/2 span)	1.00	1.00	1.02	1.03	—	—	—
	5 (2/3 span)	0.95	0.96	1.00	1.02	—	—	—
	Average	0.97	0.99	1.01	1.03	—	—	—
	Theoretical	0.95	0.98	1.02	1.05	—	—	—
2	2	1.41	1.29	1.18	1.03	0.86	0.73	0.64
	3	1.39	1.29	1.16	0.99	0.89	0.73	0.65
	4	1.41	1.30	1.18	0.98	0.86	0.74	0.64
	5	1.42	1.31	1.14	1.01	0.88	0.72	0.63
	Average	1.41	1.30	1.16	0.98	0.87	0.73	0.64
	Theoretical	1.42	1.28	1.13	1.00	0.84	0.70	0.60
1 (Edge Beam)	2	1.70	1.40	1.18	0.94	0.80	0.63	0.46
	3	1.70	1.39	1.21	0.99	0.84	0.71	0.51
	4	1.75	1.42	1.21	0.98	0.84	0.68	0.49
	5	1.68	1.41	1.21	0.91	0.85	0.73	0.54
	Average	1.71	1.40	1.20	0.96	0.84	0.69	0.50
	Theoretical	1.72	1.42	1.17	0.95	0.77	0.60	0.43

by a change in the longitudinal position of the load and the distribution at all sections was virtually identical for a given position of the load. This confirmed the assumption of the distribution coefficient analysis that the distribution coefficients are identical for all transverse sections. It is important to note that the value of α used in the analysis of the bridge contained values of i_o and j_o which were calculated for a single cell in each direction from the membrane formula $i_o = \frac{4A^2}{p\oint \frac{ds}{t}}$ where p is the spacing of the webs. If the actual torsional stiffness per unit length of the multi-webbed box had been used a value of α exceeding unity would have been obtained which is not admissible.

The comparison between the theoretical and the experimental coefficients K for the longitudinal bending moment is made in Table 10, a satisfactory agreement being obtained.

The transverse moments were too small and too greatly affected by Poisson's ratio for a comparison to be made with theory. A full investigation of transverse moments was made subsequently on a slab bridge. The results of these tests are discussed elsewhere in the paper.

(d) *The distribution of deflection in a continuous grillage.*

The distribution of deflection was investigated for various conditions of loading on the two-span continuous grillage shown in Figure 9. The

TABLE 10

Comparison between the theoretical and the experimental distribution coefficients, K, for longitudinal bending moments with load at mild-span

Load Position	Beam Position						
	1	2	3	4	5	6	7
1 Experimental	1.61	1.38	1.11	1.01	0.80	0.78	0.61
Theoretical	1.72	1.43	1.17	0.95	0.77	0.59	0.43
2 Experimental	1.46	1.32	1.15	1.00	0.89	0.77	0.67
Theoretical	1.43	1.28	1.13	0.98	0 84	0.70	0.59
3 Experimental	1.18	1.13	1.05	1.00	0.95	0.89	0.84
Theoretical	1.16	1.12	1.09	1.02	0.93	0.85	0.76
4 Experimental	0.98	1.00	1.03	1.04	1.03	0.99	0.97
Theoretical	0.95	0.98	1.02	1.05	1.02	0.98	0.95

grillage consisted of four equal precast beams 13 ft 4 in. in length with a cross-section 4 in. × 2 in. and prestressed to a uniform stress of 1,000 lb/sq. in. The beams were connected by a series of diaphragms at the supports and at the $^1/_4$, $^1/_2$ and $^3/_4$ - sections of each span. The transverse prestress was 800 lb/sq. in. The joints between the beams and diaphragms were carefully made so that the form of distribution was influenced by the torsional properties of the members. The load was invariably applied at the centre of a span, one or two spans being loaded. The use of a

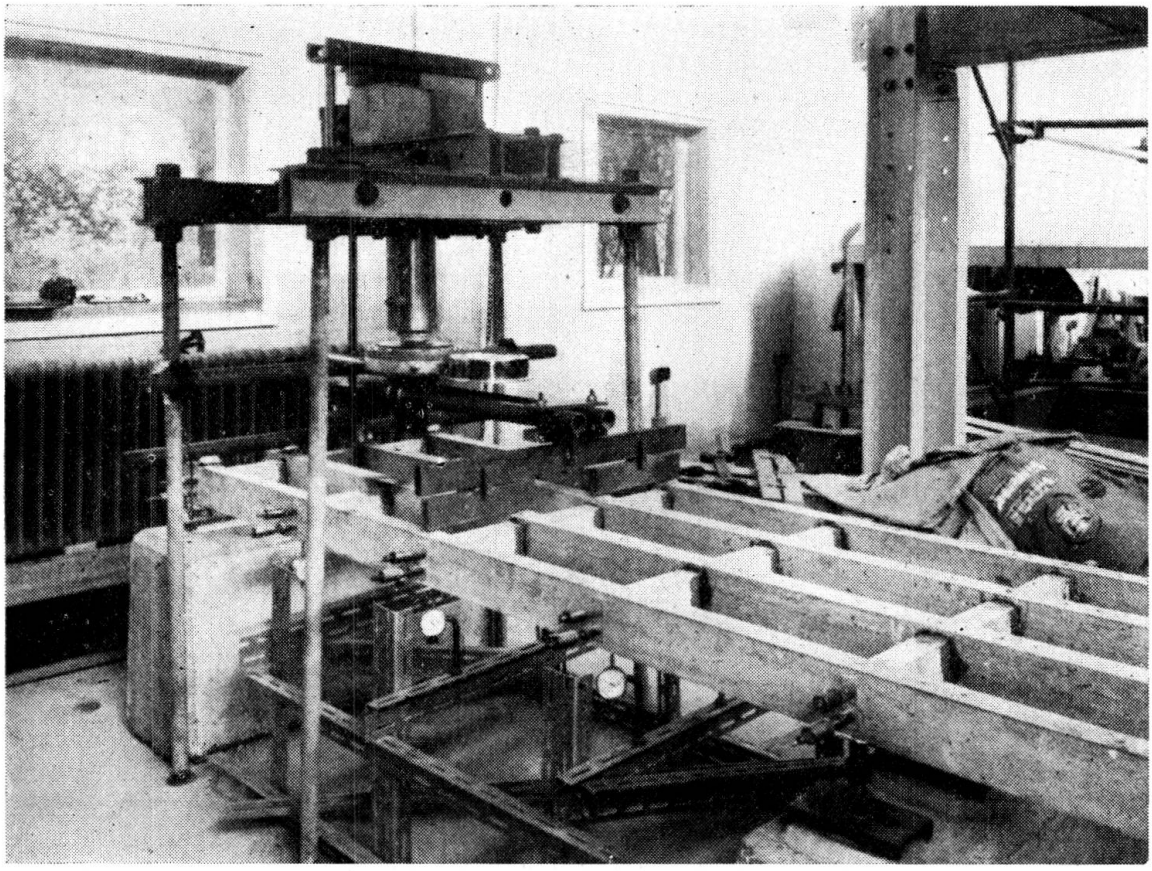

FIG. 9. Continuous grillage showing testing arrangement

lever device increased the sensitivity of loading in the ratio 5:1, whilst by incorporating knife edge connexions in the loading device equal loads were ensured in each beam.

By loading all the beams in one span equally the «mean» deflection profile was found for various loads. Allowing for measured settlement at the mid-support the value of Young's modulus E was 5.76×10^6 lb/sq. in.

A comparison between the theoretical deflections and the experimental values in the loaded span when only one span was loaded is made in the Figures 10 and 11. The theoretical lines were obtained from the analytical

coefficients, K_α found from the interpolation $K_\alpha = K_0 + (K_1 - K_0)\sqrt{\alpha}$ and the measured «mean» deflections. An average accuracy of 2 per cent was obtained, the distribution at the $^1/_4$, $^1/_2$ and $^3/_4$-span sections being virtually equal.

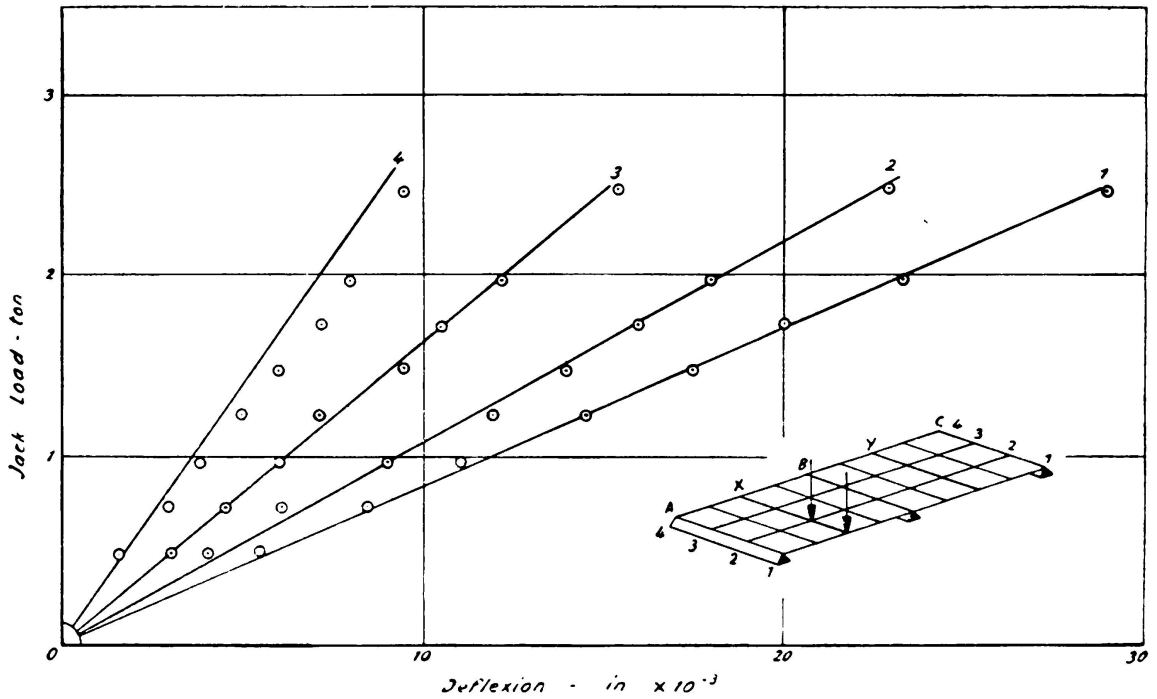

FIG. 10. Deflections along section X for single span loading

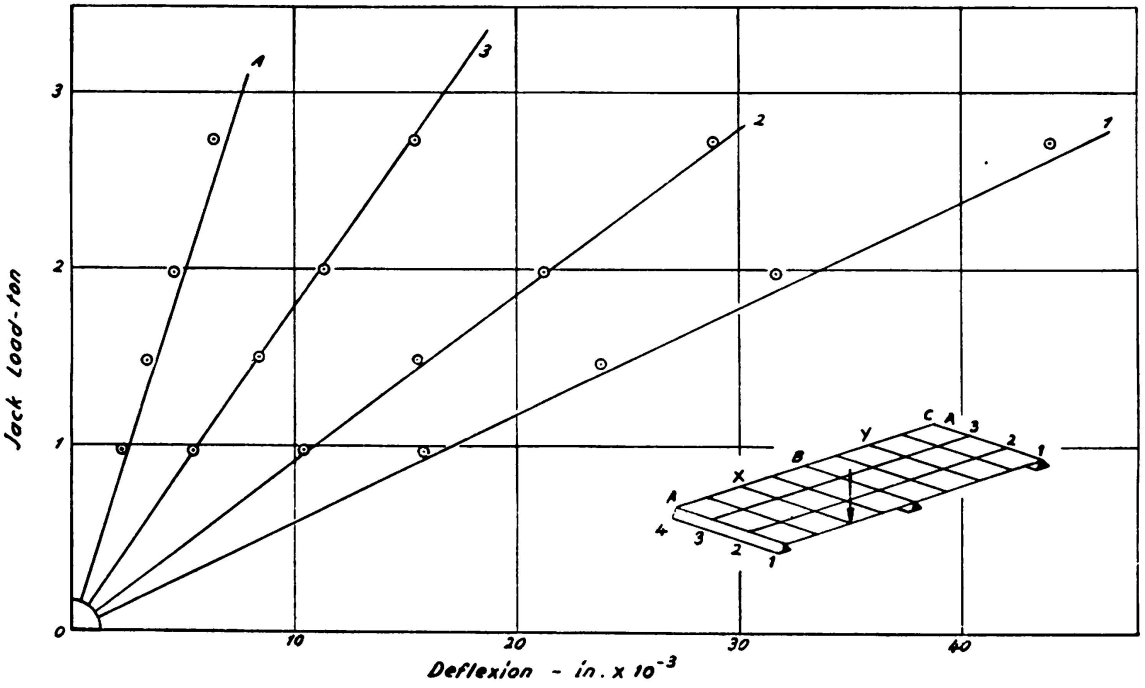

FIG. 11. Deflections along section X for single span loading

The distribution in the unloaded span is shown in Figures 12 and 13. This distribution was much more efficient than the analytical distribution and seemed to be independent of the eccentricity of the load. The deflection of each beam tended to be equal and the average of the these deflections was equal to the «measured» mean deflection.

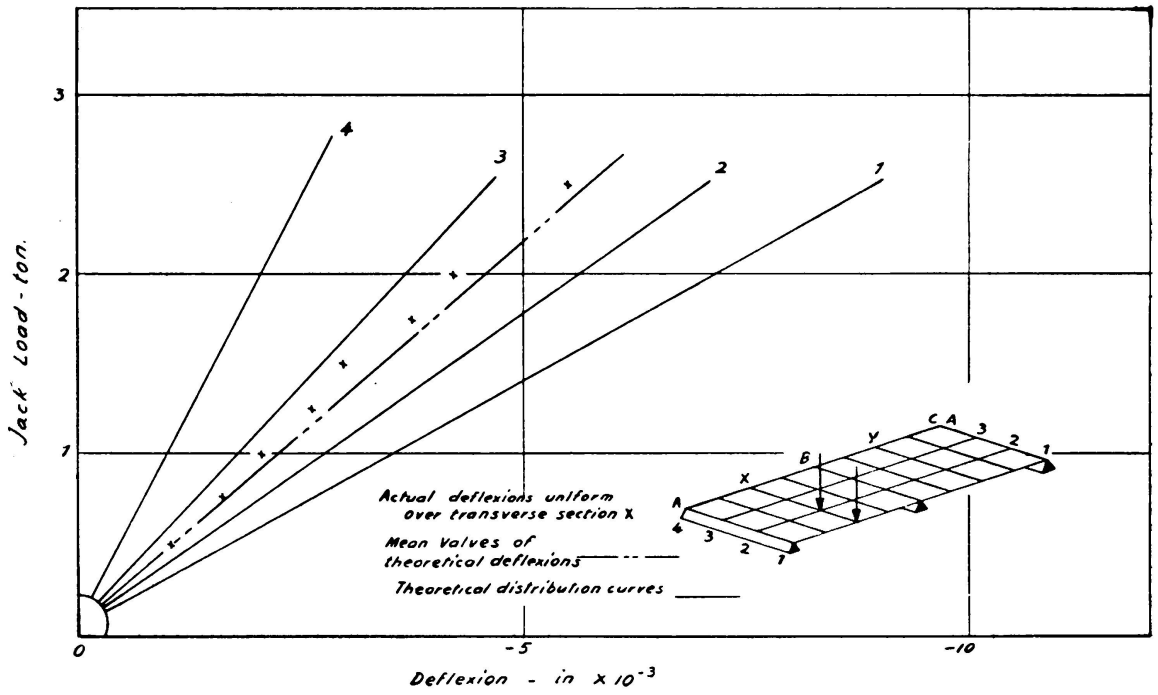

FIG. 12. Deflections along section Y for single span loading

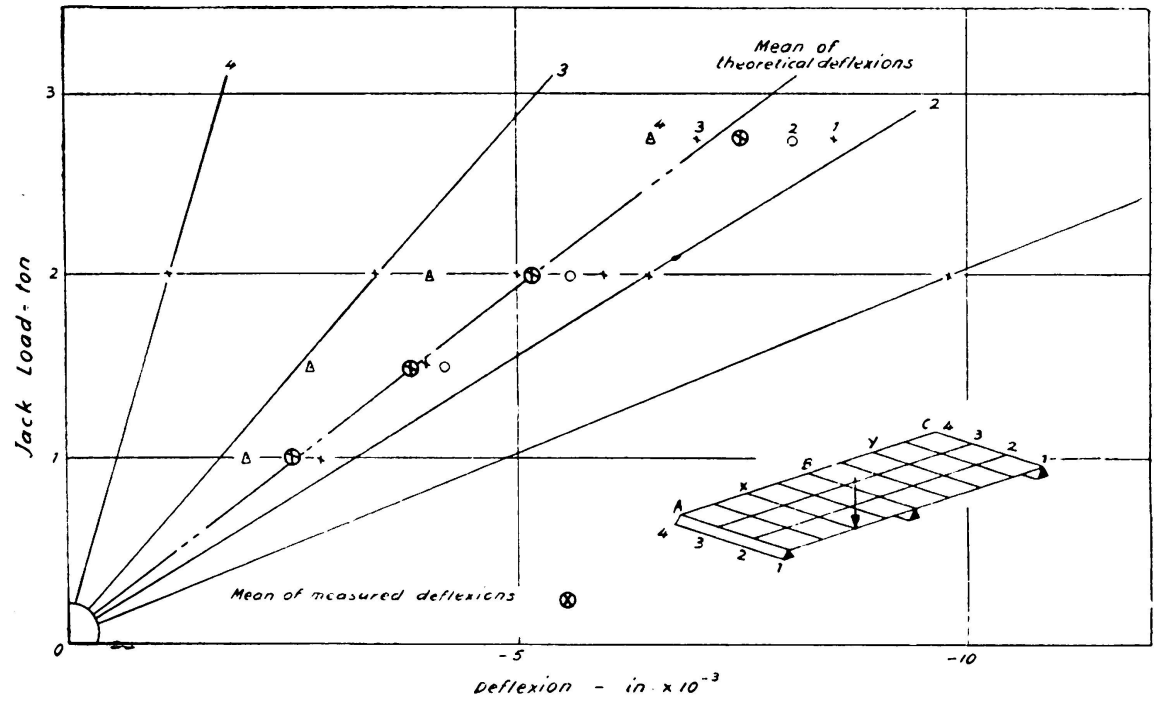

FIG. 13. Deflections along section Y for single span loading

This behaviour occurred because the torsional properties of the support diaphragms were active in redistributing the unequal bending moments at the support. Naturally differential deflections were not possible there and the result was that the deflection of the beams in the unloaded span were almost equal. It follows that by sufficiently increasing the torsional stiffness of the internal support diaphragms the deflections of all beams in the unloaded span will be equal to the «mean» deflection irrespective of the load eccentricity in the loaded span whilst if these diaphragms were omitted the distribution would be equal to the analytical distribution and would be equal in both spans.

The distribution in any span when both spans were loaded was found by superposing the distribution due to the load on that span on to the distribution as an unloaded span caused by the other load. The comparison between some of these results and the experimental values is made in Figure 14, which shows the high degree of accuracy obtained.

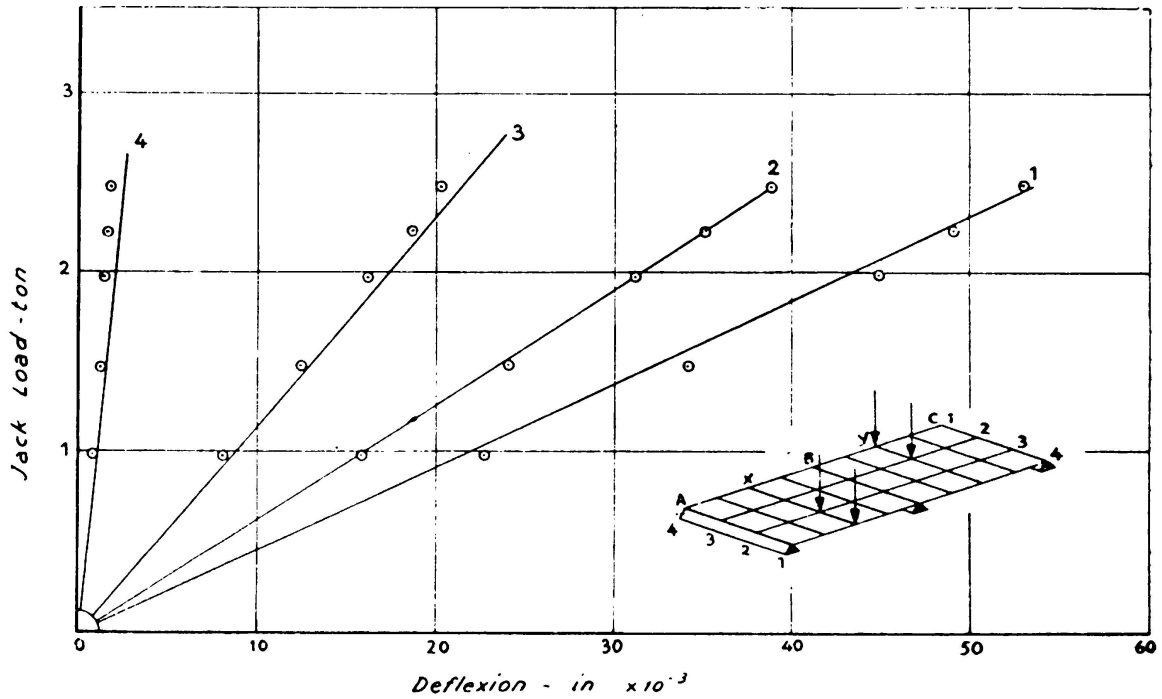

FIG. 14. Deflections along section X and Y for two span loading

In none of the previous tests was the working load of either the beams or the diaphragms exceeded.

A test to failure was made using the load of Figure 14. The working load for each span was calculated to be 960 lb. Visible cracking of the edge beams occurred at a load of 1,500 lb. The structure failed in combined bending and torsion at mid-span and at the mid-support at a load of 3,400 lb. The load factor was therefore, 3.49 and the factor of safety against cracking was 1.52. The diaphragms suffered no damage whatsoever. A subsequent analysis using the μ -coefficient solution showed, in fact, that the bridge was highly over-prestressed transversely for working conditions and that the prestress that was required for a

balanced design under the worst conditions of loading for transverse bending, i. e. the two inner beams loaded, was only 300 lb/sq. in.

It is noted that in the calculation of θ the actual length of span was used and not the effective length.

(e) *Beam and slab bridges in perspex.*

This series of tests was primarily directed at finding the correct interpolation to be given to α, the torsional parameter, to be consistent with the assumptions of analysis in bridge structures intermediate between a no-torsion grillage and a full torsion slab, and to establish the validity of the interpolation formula $K_\alpha = K_o + (K_1 - K_o)\sqrt{\alpha}$ where K_1 are the Massonnet coefficients for a slab and K_o are the Guyon coefficients for a no-torsion grillage.

A small model Tee-beam bridge, of 18 in. span and 12 in. width, was constructed in perspex and the number of transverse diaphragms was varied from zero to three equally spaced in the span. For each case the load distribution characteristics for deflections were obtained by applying a single concentrated load on the mid-span section (Figure 15).

To carry out the theoretical analysis of the bridge, it was necessary to determine the value of Young's modulus and the shear modulus of the material. Separate tests on a beam of perspex subjected to flexure and torsion yielded the results $E = 3.884 \times 10^5$ lb/in^2.; $G = 1.556 \times 10^5$ lb/in^2. and hence Poisson's ratio, ν, $= 0.248$. The method of determining the torsional parameter, α, in the theoretical analysis was to obtain the torsional rigidities in the longitudinal and transverse directions by taking the true torsional rigidity for the webs diaphragms and one-half the true value for the slab or flange, i. e. $\frac{Gh^3}{6}$ instead of $\frac{Gh^3}{3}$, to allow for the effect of continuity. Full details of the dimensions of each model and the theoretical flexural and torsional parameters are given in Table 11. In the case of a single central diaphragm, θ and α were determined for assumptions of the complete span and distance between diaphragms (central and end) as the flange width in the transverse direction. A comparison of the theoretical and experimental distribution factors is also given in Table 11.

The agreement between the theoretical and experimental values is very good, especially since the negative values at the edges of the bridge are in accord. In previous tests on bridge models the discrepancy at the edges was found to be more marked. The greater number of load positions considered for bridge deck No. 2 was to determine the correct assumption regarding the transverse flange width to be used in the theoretical analysis. Very little difference exists between the two sets of theoretical values though the assumption of diaphragm spacing as the flange width appears to give slightly better estimates of the values of K. However to ensure the validity of the fundamental assumptions on which Massonnet's analysis is based, namely, that the bridge deck system is reduced to an equivalent continuous pseudo-slab, it is necessary to consider the

TABLE 11

Main dimensions and properties of the tee-beam models

Rib thickness = 0.167 in. Longitudinal rib spacing = 2 in. Slab thickness = 0.182 in.
Slab width = 12 in. Rib depth = 1.313 in.

Transverse diaphragms at supports in all cases

Bridge deck No.	1.	2.		3.
Span = 2a	17.8108	17.8108		17.8108
Width = 2b	12	12		12
No. of longitudinal beams	6	6		6
No. of transverse diaphragms	0	1		3
Flexural stiffness/unit width = Ei	0.05448E	0.05448E		0.05448E
		(a)	(b)	
Flexural stiffness/unit width = Ej	0.000502E	0.008714E	0.0141714E	0.02923E
	1.09	0.53	0.48	0.39
Torsional stiffness/unit width = Gi_o	0.002024G	0.002024G	0.002024G	0.002024G
Torsional stiffness/unit length = Gj_o	0.0010084G	0.0011192G	0.0010620G	0.0014625G
	0.1173	0.029	0.0232	0.0176

Theoretical and experimental distribution factors

Position on section		-b	-3b/4	-b/2	-b/4	0	b/4	b/2	3b/4	b
Bridge deck No. 1	Theoretical	- 0.33	0.16	0.53	1.23	1.92	2.09	1.49	0.66	- 0.14
Load at b/6	Experimental	- 0.18	0.08	0.54	1.23	1.99	2.01	1.34	0.72	0.23
Bridge deck No. 2	Theoretical (a)	0.24	0.50	0.77	1.05	1.26	1.32	1.25	1.14	0.99
Load at b/6	Theoretical (b)	0.30	0.53	0.78	1.03	1.22	1.27	1.23	1.19	1.13
	Experimental	0.33	0.57	0.77	0.98	1.20	1.29	1.27	1.18	1.07
Loat at b/2	Theoretical (a)	- 0.35	- 0.04	0.30	0.66	1.01	1.39	1.74	1.96	2.12
	Theoretical (b)	- 0.35	- 0.04	0.31	0.67	1.00	1.39	1.72	1.97	2.18
	Experimental	- 0.21	0.09	0.38	0.67	0.99	1.33	1.72	1.95	2.05
Load at 5 b/6	Theoretical (a)	- 0.81	- 0.47	- 0.14	0 24	0.70	1.31	2.02	2.86	3.65
	Theoretical (b)	- 0.69	- 0.43	- 0.15	0.28	0.75	1.34	2.04	2.86	3.54
	Experimental	- 0.87	- 0.52	- 0.14	0.28	0.81	1.37	2.04	2.93	3.55
Bridge deck No. 3	Theoretical	0.41	0.57	0.77	0.98	1.13	1.20	1.21	1.25	1.26
Load at b/6	Experimental	0.51	0.61	0 76	0.96	1.12	1.19	1.20	1.20	1.18

(b) Distance between diaphragms considered as flange width
(a) Span considered as transverse flange width

diaphragm spacing as the transverse flange width. The value of α determined by the process outlined above yields theoretical values of K which are in excellent agreement with the experimental values.

The investigations have shown that the interpolation formula $K_\alpha = K_o + (K_1 - K_o)\sqrt{\alpha}$ can be used to determine the distribution of load in a uniform bridge structure which is neither a slab nor a simple grillage.

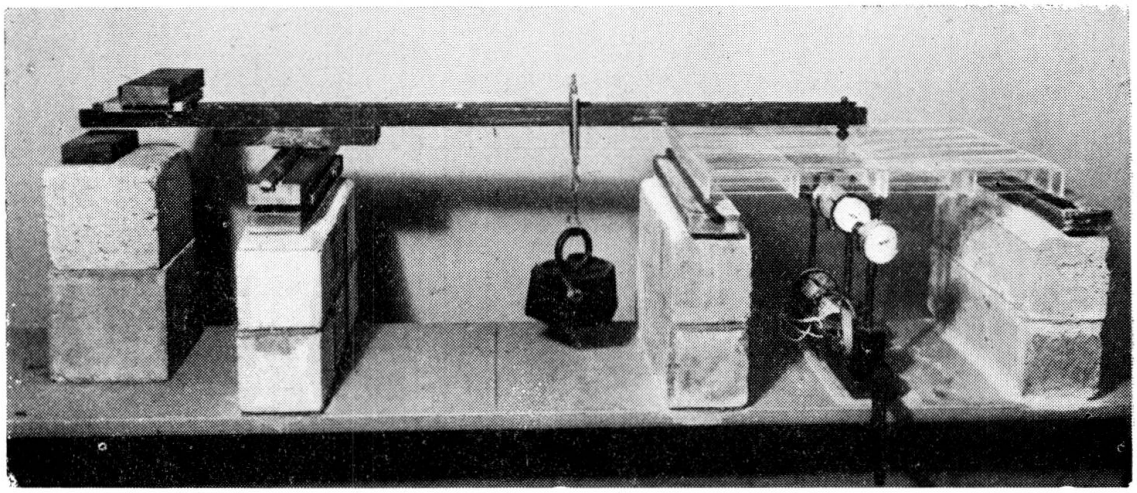

FIG. 15. Tee-beam bridge under test

The value of α for a beam and slab bridge is determined correctly if the torsional quantities Gi_o and Gj_o are equal to the sums of the true torsional stiffnesses of beams or diaphragms and one-half the true torsional stiffness of the slab.

In determining θ and α for a beam and slab bridge the actual flange width between the main beams, in the longitudinal direction, and the diaphragms, in the transverse direction, should be used and not the effective flange widths laid down by various codes of practice.

REFERENCES

1. WESTERGAARD, H. M. — *Computation of stresses in bridge slabs due to wheel loads.* Public Roads. Washington. 1930. Vol. 11. No. 1. March. pp 1-23.
2. MORRIS, C. T. — *Concentrated loads on slabs.* Ohio State University Studies. Engineering Series. 1933. Vol. 2. No. 6. November. 20 pp.
3. NEWMARK, N. M. — *A distribution procedure for the analysis of slabs continuous over flexible beams.* University of Illinois Bulletin.
4. RICHART, F. E. and KLUGE, R. W. — *Tests on reinforced concrete slabs subjected to concentrated loads.* Univertsity of Illionois Bulletin. Urbana. 1939. Vol. 36. No. 85. 75 pp.
5. JANSSONIUS, G. F. — *Nieuwe Vereffeningsmethoden voor het Berelenen van Balkroosters.* (New relaxation methods for calculation of grid frameworks). Delft. 1948. Thesis for the degree of doctor of engineering at the Technical Highschool at Delft.

6. HETENYI, M. — *A method for calculating grillage beams.* S. Timoshenko 60th Anniversary volume. New York. 1938. pp 60-72.
7. PIPPARD, A. J. S. and de WAELE, J. P. A. — *The loading of interconnected bridge girders.* Journal of the Institution of Civil Engineers. London. 1938. November. Vol 10. No. 1. pp 97-114.
8. LEONHARDT, E. and ANDRÄ, W. — *Die veremfachte Trägerrostberechnung.* (The calculation of grillage beams). Julius Hoffman Press. Stuttgart. 1950.
9. GUYON, Y. — *Calcul des ponts larges à poutres multiples solidarisées par les entretoises.* (The calculation of wide multiple beam bridges with diaphragm stiffeners). Annales des Ponts et Chaussées. Paris. 1946. September-October, pp 553-612.
10. GUYON, Y. — *Calcul des ponts-dalles.* Annales des Ponts et Chaussées. Paris. 1949. No. 5. September-October. No. 6. November-December.
11. MASSONET, C. — *Méthode de calcul des ponts à poutres multiples tenant compte de leur résistance à la torsion.* (A method for the calculation of multiple beam bridges taking into account their torsional resistance). Publications. International Association for Bridge and Structural Engineering. Zurich. 1950. Vol. 10. pp 147-182.
12. JENSEN, V. P. and ALLEN, J. W. — *Studies of highway skew slab bridges with curves.* Part. 1. Results of analysis. University of Illinois Bulletin. Urbana. 1947. Vol. 45. No. 8. 62 pp.
13. GOSSARD, M. L. and SIESS, C. P., NEWMARK, N. M. and GOODMAN, L. E. — *Studies of highway skew slab bridges curbes.* Part 2. Laboratory Research. University of Illinois Bulletin. Urbana. 1950. Vol. 47. No. 79 pp.
14. ROWE, R. E. — *A load distribution theory for bridge slabs allowing for the effect of Poisson's ratio.* London. Magazine of Concrete Research. 1955, vol 7, N° 20, pp 69–78.

SUMMARY

After a short discussion of the bridge loading problem in Great Britain a brief survey is given of the methods available for the elastic analysis of right bridges subjected to concentrated loads. Mention is made of the determination of transverse moments in the distribution coefficient method, originally due to Guyon, and the expression is given for the calculation of the transverse moment coefficients in slabs in which the value of Poisson's ratio has been included.

The main portion of the paper is devoted to the description of a number of tests on bridges and bridge models and a discussion of the results and their comparison with the distribution coefficient calculations. The bridges tested were two-way prestressed concrete slab models, a small prestressed concrete highway bridge and a one-quarter scale model, a multi-webbed box model in xylonite, a two-span prestressed concrete beam grillage and a beam and slab bridge model in perspex.

ZUSAMMENFASSUNG

Nach einem kurzen Hinweis auf das Problem der Brückenbelastung in Grossbritannien geben die Verfasser einen Ueberblick über die verschiedenen Verfahren, welche für die Bestimmung der Elastizitätsgleichungen bei geraden Brücken unter punktförmigen Einzellasten zur Anwendung kommen. Die Bestimmung der Momente in der

Querrichtung folgt der ursprünglich von Guyon entwickelten Methode mit den Verteilkoeffizienten, wobei zur Berechnung dieser Koeffizienten die Poisson'sche Zahl berücksichtigt ist.

Der Hauptteil dieser Arbeit ist der Besprechung einer Anzahl Versuche, welche an Brücken und Modellen vorgenommen wurden und dem Vergleich dieser Versuchsergebnisse mit den rechnerisch bestimmten Verteilungswerten gewidmet. Bei den untersuchten Brücken handelte es sich um 3 in Längs- und Querrichtung vorgespannte Beton-platten--Modelle, eine kleine vorgespannte Strassenbrücke und ein Modell im Masstab 1:4, ein Modell eines mehrgurtigen Kastenträgers aus Xylonit, einen über zwei Spannwerten vorgespannten Trägerrost aus Eisenbeton und ein Plattenbalken-Brückenmodell aus Perspex.

RESUMO

Depois de uma breve discussão do problema das cargas sobre as pontes na Grã-Bretanha, o autor examina ràpidamente os métodos disponíveis para o cálculo elástico de pontes rectas submetidas a cargas concentradas. Menciona-se a determinação dos momentos transversais pelo método dos coeficientes de distribuição de Guyon, e indica-se a expressão que permite calcular os coeficientes dos momentos transversais em lages entrando em conta com o valor do coeficiente de Poisson.

A parte principal da contribuição trata da descrição de uma série de ensaios efectuados em pontes e em modelos de pontes e da discussão dos resultados e sua comparação com os obtidos pelo método dos coeficientes de distribuição. Os ensaios efectuaram-se sobre modelos de pontes com lage em betão preesforçado em dois sentidos, uma pequena ponte--estrada de betão preesforçado e um modelo da mesma ponte à escala de 1/4, um modelo de viga-caixão de alma múltipla de xilonite, um reticulado de vigas sobre três apoios de betão preesforçado e um modelo de ponte com viga e lage de perspex.

RÉSUMÉ

Après une courte discussion du problème des charges sur les ponts en Grande-Bretagne, l'auteur donne un bref aperçu des méthodes disponibles pour le calcul élastique de ponts droits soumis à des charges concentrées. Il mentionne la détermination des moments transversaux par la méthode des coefficients de distribution dûe à Guyon et donne l'expression permettant de calculer les coefficients des moments transversaux dans les dalles en tenant compte du coefficient de Poisson.

La partie principale du mémoire s'occupe de la description d'une série d'essais effectués sur des ponts et des modèles de ponts et de la discussion des résultats et de leur comparaison avec ceux obtenus par la méthode des coefficients de distribution. Les essais ont porté sur des modèles de dalles en béton précontraint dans les deux directions, un petit pont-route en béton précontraint et son modèle à l'échelle 1/4, un modèle de poutre en caisson à âme multiple en xilonite, un réticule de poutres sur trois appuis en béton précontraint et un modèle de pont à poutre et dalle en perspex.

IIc2

Die statische Berechnung von zylindrischen Stahlbeton--Behältern auf Grund der Bruchtheorie

Cálculo estático baseado na teoria da rotura de um reservatório cilíndrico de betão armado

Calcul statique fondé sur la théorie de la rupture d'un réservoir cylindrique en béton armé

Statical calculation based upon the collapse theory of a reinforced cylindrical concrete tank

DR. I. MENYHÁRD
Budapest

1. *Problemstellung.*

Die statische Berechnung von gekrümmten dünnen Platten — Schalen — ist eines der schwierigsten Probleme der Elastizitätslehre. Die statische Berechnung von Trägern und Platten aus plastischem Material auf Grund der Bruchtheorie ermöglicht aber eine bedeutende Vereinfachung im Vergleich zu den Untersuchungen der Elastizitätslehre.

Die Anwendung der Bruchtheorie wird durch den Umstand erschwert, dass der Bruch der Schalen sich oft als Folge der ungenügenden Stabilität ergibt. Wenn aber unter den Schnittkräften der Schale die Druckraft eine untergeordnete Rolle spielt, verliert die Frage der Stabilität seine Wichtigkeit und hiermit kann die Bruchtheorie schon auf Grund unserer heutigen Kenntnisse zur Anwendung kommen.

Um dies zu illustrieren, werden wir im Folgenden mit Hilfe der Bruchtheorie die statische Berechnung eines auf der unteren und oberen Fläche teilweise eingespannten kreiszylinderförmigen Flüssigkeitsbehälters durchführen. Die Beanspruchungen, die hierbei eine Rolle spielen, sind die Biegungsmomente in Richtung der Erzeugenden und die auf diese Richtung lotrechten Zugkräfte (Ringkräfte).

Hierbei werden wir uns auf die selben Annahmen stützen, wie die dies bezügliche Literatur. Diese Annahmen beziehen sich einerseits auf das in der Bruchtheorie eine bedeutende Rolle spielende Bruchbild, anderseits auf diejenigen Biegungsmomente, die in den Querschnitten beim

Bruch auftreten, die sogenannten Bruchmomente. Die Annahmen sind die folgenden:

a.) Die von den Bruchlinien begrenzten Plattenteile (bezw. Flächenteile) bleiben nach der plastischen Deformation eben (bezw. von unveränderter Krümmung).

b.) Die die Bruchlinien kreuzenden Armierungseisen fliessen und bei Platten mit konstanter Dicke und gleichmässig verteilter Armierung sind die Bruchmomente entlang dieser Linien ebenfalls konstant und unabhängig von der Grösse der plastischen Deformation.

c.) Man schliesst diejenige Deformationen aus, für welche die Dehnung der Armierung die Verfestigungsgrenze überschreitet d. h. es soll keine grössere Stahlspannung als diejenige, die im Fliessbereich entstehen.

2. *Die statische Berechnung auf Grund der Bruchtheorie.*

Der Mantel des in Abb. 1a schematisch dargestellten kreiszylinderförmigen Eisenbetonbehälters ist mit der Bodenplatte und mit dem am oberen Rand befindlichen Versteifungsring verbunden. Die Bodenplatte und der Versteifungsring sichern die Ränder des Mantels gegen eine horizontale Verschiebung. Beide Elemente sind zur Aufnahme eines

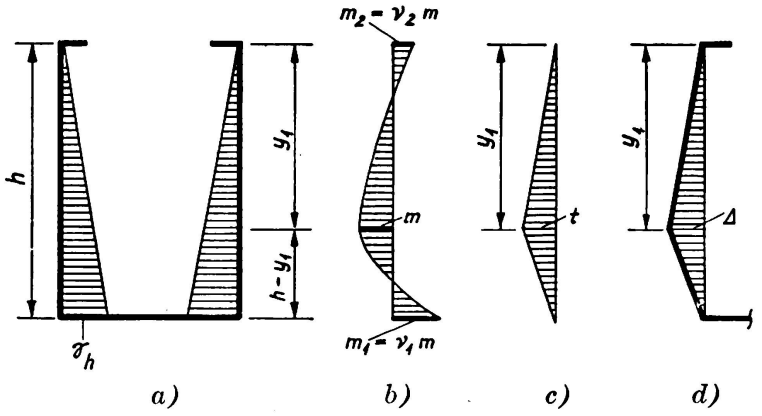

FIG. 1

negativen, vom Mantel übertragenen Biegemomentes von bestimmter Grösse fähig. Als gegebene äussere Belastung wirkt auf den Mantel ein dreieckförmig verteilter hydrostatischer Druck (Abb. 1a). Die Seitenwand des Behälters ist in der Richtung der Erzeugenden mit einer äusseren und inneren Bewehrung versehen, und ist fähig, ein positives Biegungsmoment von bestimmter Grösse m und Einspannungsmomente $m_1 = \nu_1 m$ bezw. $m_2 = \nu_2 m$ an dem unteren bzw. oberen Rande des Mantels aufzunehmen (Abb. 1b).

Der Mantel ist auch in tangentialer Richtung bewehrt. Diese Bewehrung dient zur Aufnahme von Ringzugkräften. Die Ringarmierung sei gemäss einem Dreieck (Abb. 1c) verteilt und so gewählt, dass die Bewehrung im Fliesszustande an der Stelle des grössten Armierungsgehaltes gerade zur Aufnahme der spezifischen Zugkraft t fähig ist. Die Spitze des Dreiecks liegt auf der später zu bestimmenden horizontalen Bruchlinie. Die Mantelfläche des kreiszylinderförmigen Behälters nimmt

beim Bruch die aus Abbildung 2 ersichtliche Form an, wobei die Erzeugenden gemäss der Abb. 1d gebrochen werden und damit verwandelt sich der Kreiszylinder in zwei sich berührende stumpfe Kegel. Die Form des Bruchbildes wird also durch die am Mantelrand und an der Stelle des grössten positiven Moments auftretenden horizontalen Bruchlinien, sowie durch die dicht (theoretisch unendlich dicht) auftretenden vertikalen Bruchlinien charakterisiert. Die Lage der horizontalen Bruchlinie ist dabei noch unbekannt. Sie sei mit dem Parameter y_1 gekennzeichnet (Abb. 2).

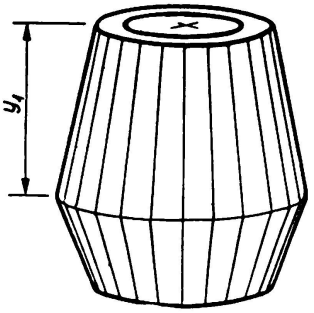

FIG. 2

Unser Endziel ist also, die statische Berechnung unter Benützung des jetzt bescriebenen Bruchbildes durchzuführen.

Als Grundlage zu dieser Berechnung diene die Tatsache, dass die äusseren Kräfte mit den inneren Kräften zusammen die Gleichgewichtsbedingungen erfüllen müssen. Die Gleichgewichtsbedingung sei durch das Arbeitsprinzip ausgedrückt, dass aussagt, dass die Arbeit L_a der äusseren Kräfte der Arbeit L_i der inneren Kräfte gleich ist. Im vorliegenden Falle ist

$$(1)\quad L_a = 2\pi r \gamma \Delta \left[\int_0^{h_1} \frac{y^2}{y_1}\, dy + \int_{y_1}^{h} \frac{y(h-y)}{h-y_1}\, dy \right] = \frac{\pi r \gamma \Delta h}{3}(y + y_1),$$

$$(2)\quad L_i = 2\pi r \Delta \left[\frac{y_1(v_1 - v_2) + h(1+v_2)}{y_1(h-y_1)}\, m + \frac{h}{3r}\, t \right].$$

Die Grössen γ, r, h, und Δ sind aus den Abbildungen 1 a-d ersichtlich.

Durch Gleichsetzen von (1) und (2) ergibt sich eine Gleichung, woraus γ sich berechnen lässt. Damit erhalten wir

$$(3)\quad \gamma = \frac{6(1+v_2)\,m}{h^3} \cdot \frac{(\eta K + 1)}{\eta(1-\eta)(\mu+\eta)} = \frac{6(1+v_2)\,m}{h^3} \cdot \frac{1}{\varrho},$$

worin

$$(4)\quad K = \frac{v_1 - v_2}{1+v_2},\quad \mu = 1 - \frac{2t}{\gamma r h},\quad \eta = y_1/h$$

und

$$(5)\quad \varrho = \frac{\eta(1-\eta)(\mu+\eta)}{\eta K + 1}$$

ist.

In der Formel (3) ist der Parameter η, welcher an Stelle von y_1 eingeführt wurde, noch unbekannt.

Die Gleichung (3) bedeutet folgendes: an einer durch η charakterisierten Stelle wird ein Biegemoment von der Grösse m (d. h. der Bruch) dann auftreten, wenn die Belastung γ den Wert (3) annimmt, (vorausge-

setzt, dass an den anderen Stellen der Biegungswiderstand hinreichend gross ist, um den Bruch zu verhindern). Da aber eine konstante Wanddicke und eine gleichmässig verteilte, vertikale Bewehrung vorausgesetzt wird und hiermit der Biegungswiderstand auch an anderen Stellen gleich m ist, wird der Bruch an jenem Ort auftreten, wo γ als Funktion von η seinen Minimalwert erreicht.

Um η zu ermitteln, muss man folglich die Gleichung

$$\frac{d\gamma}{d\eta} = 0$$

benützen, oder ausführlich geschrieben und nach K aufgelöst

$$K = \frac{\eta(2-3\eta)+\mu(1-2\eta)}{\eta^2(2\eta+\mu-1)} \quad . \tag{6}$$

Die geometrische und statische Grössen nehmen beim Bruch solche Werte an, welche die Gleichungen (3), (6) erfüllen. Man wird diese zwei Gleichungen, entsprechend der gegebenen Aufgabe, in einer modifizierten Form verwenden. Sind z. B. ausser den geometrischen Grössen die Werte K und μ gegeben und will man m berechnen, so schreiben wir die Gleichung (3) in folgender Form an:

$$m = \frac{\gamma\, h^3}{6\,(1+\nu_2)} \cdot \frac{\eta(1-\eta)(\mu+\eta)}{\eta K+1} = \frac{\gamma\, h^3}{6\,(1+\nu_2)}\,\rho \tag{7}$$

Wir haben also zwei Gleichungen, nämlich die Gleichung (6) und die Gleichung (3) oder (7). Die erste von diesen ist von dritten Grade in η. Das Auflösen der Gleichungen wird durch die Benützung der Abbildungen 3a und 3b erleichtert. In Abb. 3a ist η als Funktion von K und μ, in Abb. 3b μ als Funktion von K und ρ dargestellt.

Beschränken wir uns auf die praktischen Fälle

$$-0{,}4 < \mu < 0{,}6 \quad \text{und} \quad 0{,}4 < K < 4 \quad ,$$

so liefern die Formeln

$$\rho = 0{,}85\,\frac{0{,}73-\mu}{(1{,}62+0{,}62\,\mu+K)\,(2{,}62-\mu)} \quad , \tag{8}$$

$$\mu = 14{,}7\,\frac{(1{,}5+K)\,\rho-0{,}226}{(1{,}5+K)\,(1{,}9+K)\,\rho+4{,}41} \quad , \tag{9}$$

$$\eta = 0{,}24\,\frac{4{,}08+\mu}{1{,}62+\mu} + 0{,}11\,\frac{1{,}5-K}{2{,}5+K}\,(0{,}75+\mu) \tag{10}$$

eine gute Näherungslösung. Punkt 3 bezieht sich auf die Benützung der Abbildungen 3a, 3b und der Formeln (8), (9), (10).

Bemerkung: Bei der Herleitung der Formel (2) haben wir den Umstand ausser Acht gelassen, dass die in den kleinen oberen und unteren Partien des zylindrischen Mantels befindliche Ringbewerhrung die Streckgrenze noch nicht erreicht und somit die Spannung hier kleiner als die Fliessspannung ist. Der infolge dieser Vernachlässigung

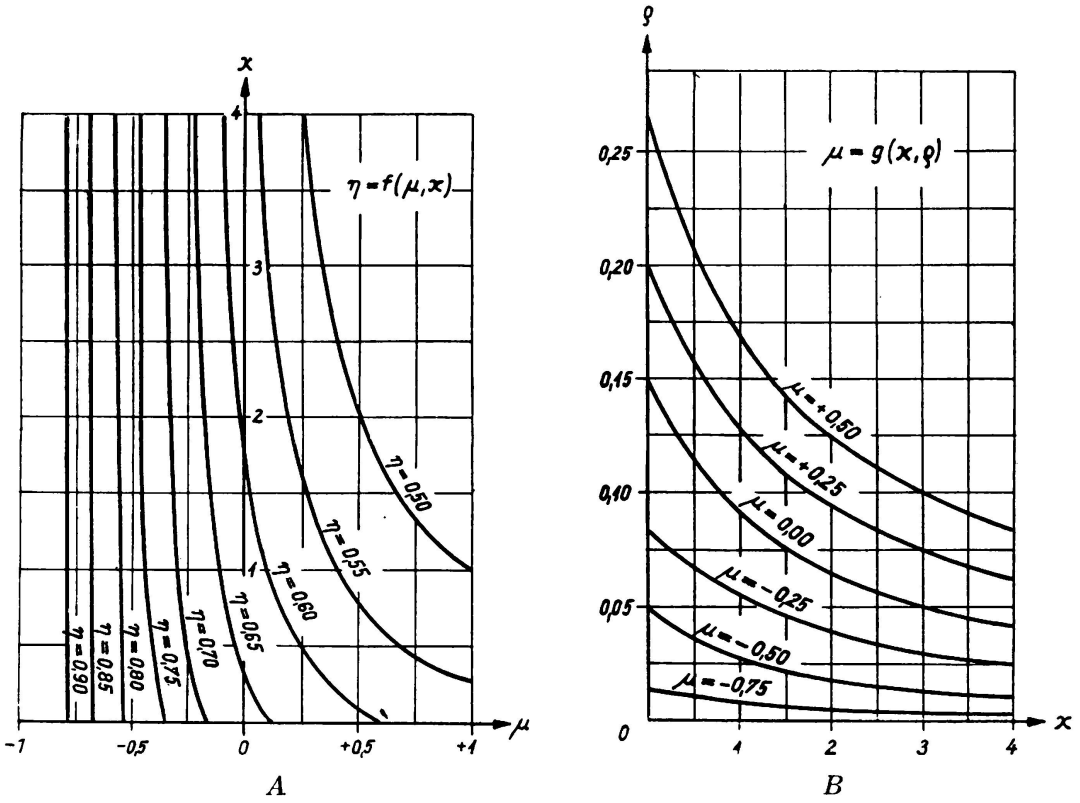

FIG. 3

entstehende Fehler in unserer Berechnung ist aber vernachlässigbar klein, da nach unserer Annahme der Armierungsgehalt der Ringbewehrung dreieckförmig variiert.

3. *Rissfreiheit. Wahl der Bewehrung.*

Für den Gebrauch der Flüssigkeitsbehälter ist die Rissfreiheit meistens eine unerlässliche, oder wenigstens wichtige Bedingung. Was das Entstehen der Haarrisse anbelangt, verhalten sich die auf Biegung beanspruchten Eisenbetonkonstruktionen wie elastische, aber gleichzeitig spröde Körper, d. h. dem Auftritt der Haarrisse geht kein plastische Formänderung voraus und die Rolle der Bewehrungsstäbe ist im Hinblick auf die Vermeidung der Haarrisse unbedeutend. Hieraus folgt, dass im Falle einer erforderlichen Rissefreiheit die Wanddicke des Behälters aus den nach der Elastizitätstheorie berechneten Beanspruchungen zu ermitteln ist, wobei auf die Zugfestigkeit des Betons Rücksicht genommen werden muss. Die Bewerung des Behälters ist vor allem deshalb

notwendig, dass in folge eines unvorgesehenen Risses kein plötzlicher Zusammenbruch entsteht. Dies ist die Sicherheitsforderung gegen Bruch.

Demgemäss kann die Stärke der Bewehrung (die Menge der Bewehrungsstäbe) auf Grund der Bruchtheorie errechnet werden.

Wie wir im Vorausgegangenen gesehen haben, werden in der Bruchtheorie — im Gegensatz zu der Elastizitätsteorie — bestimmte Werte der Beanspruchungen, in unserem Falle die Kräfte in der Ringrichtung und die Biegungsmomente in der Richtung der Erzeugenden, durch funktionelle Zusammenhänge ersetzt. Dies bedeutet, dass wir aus einer Menge von Bewehrungssystemen auswählen können. Wir könnten z. B. im Sinne der Bruchtheorie, einen Flüssigkeitsbehälter ohne Ringbewehrung entwerfen; in diesem wird die Belastung nur von der Längsbewehrung getragen. Analog könnten alle Kräfte von der Ringbewehrung aufgenommen und sämtliche, den Biegungsmomenten entsprechende Längsbewehrungsstäbe weggelassen werden. Selbstverständlich sind solche extreme Anordnungen der Bewehrung nicht vorteilhaft und es scheint zweckmässig das folgende Verfahren anzuwenden. Nachdem die Wanddicke des Mantels aus der Bedingung der Rissefreiheit schon ermittelt worden ist, soll die Menge der Längsbewehrungsstäbe einerseits dem in den offiziellen Stahlbetonbestimmungen festgesetzten Wert entsprechen, anderseits den aus konstruktiven Gründen erforderlichen Werten genügen. (So beträgt z. B. — nach den ungarischen Bestimmungen — im Falle der Anwendung eines Betons mit 200 kg/cm² Würfelfestigkeit und einem Stahl mit einer Streckgrenze von 24 kg/mm² die minimale Bewehrung an der Stelle des grössten Biegungsmoments, 0,25 % der Betonfläche). Das grösste Biegungsmoment tritt im Allgemeinen im unteren Einspannungsquerschnitt der Mantelwand auf, demgemäss wählt man als vertikale Bewehrung auf der inneren Seite der Mantelfläche das in den Bestimmungen vorgeschriebene Mindestmass.

Was die an der äusseren Seite des Mantels anzubringende Bewehrung anbelangt, ist es zweckmässig diese nicht kleiner als die Hälfte der Minimalbewehrung anzunehmen. Und wenn auch schon jene Frage entschieden ist, ob am oberen Rande des Mantels eine Einspannung bis zu einem gewissem Grade berücksichtigt wird, bleibt dann nur noch die Lage der mittleren Bruchlinie und der notwendige Armierungsgehalt der Ringbewehrung zu bestimmen.

Nach den obigen Ausführungen wird der Rechnungsgang in einem Falle, wo der Mantel des Behälters unten eingespannt, oben frei drehbar und unverschieblich ist, der Folgende sein:

Die konstante Manteldicke wird so gewählt, dass die Forderung der Rissfreiheit erfült ist. Verwenden wir gemäss der vorherigen Erörterungen eine, den Vorschriften entsprechende minimale Längsbewehrung auf der innerer Seite des Mantels, und deren Hälfte auf ihrer äusseren Seite, so haben wir mit den Bezeichnungen der Abb. 1b

$$\nu_1 = 2 \quad ; \quad \nu_2 = 0$$

und gemäss (4)

$$K = \frac{\nu_1 - \nu_2}{1 + \nu_2} = 2 \quad ,$$

weil die Biegetragfähigkeit $m_1 = v_1 m$ des Mantels an seinem unteren Rande doppelt so gross ist, wie seine Biegetragfähigkeit für positive Momente. Aehnlicherweise ist $m_2 = v_2 m$ gleich Null.

Die letztere Behauptung folgt aus der Voraussetzung, dass der obere Mantelrand keinen Biegungswiderstand leistet.

Aus der Manteldicke und aus der Stärke der äusseren Bewehrung lässt sich die positive Biegetragfähigkeit m berechnen, hieraus und aus Formel (7) ergibt sich

$$\rho = \frac{6m\,(1 + v_2)}{\gamma\, h^3} \qquad (11)$$

Wenn man ρ und K kennt, kann man den Wert μ aus Abb. 3a ablesen oder aus der Formel (9) berechnen, woraus der Betrag der Spezifischen Ringkraft gemäss Formel (4) sich zu

$$t = \frac{\gamma\, r\, h\,(1 - \mu)}{2} \qquad (12)$$

ergibt (Abb. 1d).

Und schliesslich ist der Wert $\eta = y_1/h$ unter Benützung von ρ und μ aus der Abb. 3b zu entnehmen oder mittels der Formel (10) zu berechnen. Damit ist die Lage der Bruchlinie, d. h. die Lage des grössten Armierungsgehaltes der Ringbewehrung bestimmt.

ZUSAMMENFASSUNG

Unter den Schalen bildet der kreiszylindriche Behälter ein klassisches Beispiel, für dessen statische Berechnung die Bruchtheorie leicht anwendbar ist, da sein Kräftespiel äusserst einfach und seine Tragfähigkeit nicht durch Knicken gefährdet ist.

Die Abhandlung beschreibt ein Verfahren für die im Titel angegebene Berechnung. Das Verfahren beruht einerseits auf der Benützung der auf den Abbildungen 1d und 2 dargestellten Bruchfiguren, anderseits auf den üblichen Annahmen der Bruchtheorie. Die kinematische Betrachtung des Bruchvorganges führt zu einer Gleichung, die das Arbeitsprinzip ausdrückt, wonach die Arbeit der äusseren Kräfte der Arbeit der inneren Kräfte gleich ist. Dieses Gleichgewichtsprinzip wird dann mit einer Minimalforderung verknüpft. Hiermit ergeben sich Gleichungen, die zur Berechnung der unbekannten statischen und geometrischen Grössen nötig sind.

RESUMO

O depósito cilíndrico constitui um exemplo clássico de um invólucro em cujo cálculo se pode empregar fàcilmente a teoria da rotura, dado que a distribuição dos esforços tem uma forma extremamente simples e que a resistência do mesmo não é afectada por discontinuidades de forma.

O autor descreve um processo de cálculo estático de um reservatório cilíndrico de betão armado. Este método baseia-se por um lado no emprego do diagrama de rotura indicado nas figuras 1d e 2, e por outro nos princípios da teoria da rotura. O estudo cinemático da rotura, permite estabelecer uma equação que traduz o princípio da igualdade dos trabalhos, pelo que o trabalho das forças interiores tem de ser igual ao das forças exteriores. Este princípio de equilíbrio tem de obedecer a uma condição de valor mínimo. Obtêm-se assim equações que permitem calcular as incógnitas estáticas e geométricas.

SUMMARY

Cylindrical tanks are classical examples of shells for the analysis of which the collapse theory can be easily used due to their very simple stress distribution and the fact that their resistance is not affected by shape discontinuity.

The author describes a method of statical analysis of a reinforced concrete cylindrical tank. This method is based on the use of the collapse diagram shown on figures 1d and 2 and on the principles of the collapse theory. The kinematic study of collapse leads to an equation expressing the principle of equality of works, by which the work of the internal forces must be equal to that of the external ones. This principle of equilibrium must obey a minimum value condition. Equations are thus obtained allowing the calculation of the static and geometric unknown quantities.

RÉSUMÉ

Le réservoir cylindrique est un exemple classique d'un voile pour le calcul duquel on peut appliquer sans difficulté la théorie de la rupture, grâce à la forme extrêmement simple de la distribution des efforts et au fait que sa résistance n'est affectée par aucune discontinuité de forme.

L'auteur décrit une méthode de calcul statique d'un réservoir cylindrique en béton armé. Cette méthode se fonde d'une part sur l'emploi du diagramme de rupture indiqué aux figures 1d et 2, et d'autre part sur les principes de la théorie de la rupture. L'étude cinématique de la rupture conduit à une équation qui traduit le principe de l'égalité des travaux, par lequel le travail des forces intérieures doit être égal à celui des forces extérieures. Le principe d'équilibre doit ensuite à une condition de valeur minimum. On obtient ainsi des équations permettant de calculer les inconnues statiques et géométriques.